JOURNAL OF PROPULSION AND POWER
Vol. 22, No. 6, November–December 2006

Detonation in Reactive Solid Particle–Gas Flow

Fan Zhang*
Defence Research and Development Canada – Suffield, Medicine Hat, Alberta T1A 8K6, Canada

DOI: 10.2514/1.18210

Nomenclature

C = transverse wave velocity, m/s
c_f = frozen sound speed, m/s
c_p = solid specific heat capacity at constant pressure, J/kg · K
D = detonation velocity, m/s
d = tube internal diameter, cm
d_p = solid particle diameter, μm
E_{cr} = critical energy for direct initiation of detonation, J
e = specific internal energy, J/kg
f_p = rate of momentum transfer between the solid and the gas phase, N/m^3
f_W = rate of momentum transfer to lateral boundaries, N/m^3
I = blast wave integral
J_p = rate of mass transfer between the solid and the gas phase, kg/m^3 · s
L_p = velocity or temperature relaxation length scale of solid phase, m
L_{1r} = ZND detonation zone thickness of gas phase, m
M = gas phase species number
$N-1$ = number of the solid phases
n_p = solid particle number density, 1/m^3
p = partial pressure, N/m^2
Q_f = final equilibrium heat release, J/kg
$Q_{\max}$ = highest attainable partial-equilibrium heat release, J/kg
Q_p = rate of heat transfer between the solid and the gas phase, J/m^3 · s
Q_W = rate of heat transfer to lateral boundaries, J/m^3 · s
q = heat release, J/kg
q_a = exothermic heat release of two irreversible gas reactions, J/kg
q_b = endothermic heat release of two irreversible gas reactions, J/kg
$q'_p J_p$ = energy release rate of all solid phases, J/m^3 · s
r = radius, cm
u = flow velocity, m/s
w = gas species reaction rate, kg/m^3 · s
x = distance in the shock propagation direction, m
α = triple point track angle, deg
γ = isentropic exponent
η = gas sonic parameter
λ = detonation cell size, m
ρ = material density, kg/m^3
σ = particle density or concentration, kg/m^3
ϕ = volume fraction equivalence
Ψ = thermicity, 1/s
ω = angular velocity, rad/s

Subscripts

CJ = Chapman–Jouguet state
cr = critical state
p = solid-phase index
1 = gas-phase index
0 = initial state

Introduction

FINE organic or metallic particles suspended in an oxidizing gas or air form a reactive particle–gas mixture with high-energy contents. Detonation in dilute reactive particle–gas mixtures has been experimentally studied extensively, including works [1–20]. A reactive particle–gas mixture can sustain a detonation wave whose propagation mechanism is dominated by a transverse wave structure. Because of the additional time scales inherent in the mass, momentum, and heat transfer between the solid particles and the gas, the transverse wave spacing of the detonation wave is much larger than that for homogeneous gas detonation waves. Consequently, deflagration-to-detonation transition (DDT) and propagation of a self-sustained detonation wave in particle–gas mixtures require a strong initiation and a large tube diameter as well as a sufficient tube length-to-diameter ratio. This, however, was by no means clear in the early studies between the 1960s and the early 1980s. Most of the experiments were conducted in rather small tubes of only a few centimeters in cross-sectional dimension by a few meters long, in which solid particles were dispersed in oxygen to increase mixture sensitivity [1,3,5–10]. The transition from deflagration to detonation observed in these experiments mainly exhibited a gradual acceleration to a quasi-steady state without the abrupt onset of an overdriven detonation accompanied by a retonation wave. The detonation velocities determined were 20–40% less than those predicted by the equilibrium Chapman–Jouguet theory. Whereas this phenomenon might be termed "quasi detonation" [21], its propagation mechanism remains a subject of current research.

Dr. Fan Zhang is a senior scientist in the Department of National Defence at Defence Research and Development Canada–Suffield and an adjunct Professor at the University of Waterloo in the Department of Mechanical Engineering. He specializes in shock waves, detonations, and explosions, more specifically in multiphase reactive flow and high energy density systems. He has made significant contributions in the areas of heterogeneous detonations in reactive solid particle-gas flow, heterogeneous explosion of metallized composite explosives, and related dense supersonic multiphase flow. He earned his doctorate in science from the University of Technology Aachen (RWTH), Germany in 1989 in mechanical engineering, and received a Borchers Medal, a Friedrich–Wilhelm Prize, and several best paper awards. He has published more than 100 refereed journal and proceedings papers, book chapters, and special issues in journals. Dr. Zhang currently serves as a member of the International Advisory Committee for the International Symposium on Shock Waves, the Executive Committee for the International Symposium on Military Aspects of Blast and Shock, and is a coeditor of the Springer Reference Library of Shock Wave Research.

Received 15 June 2005; revision received 21 January 2006; accepted for publication 25 January 2006.

*P.O. Box 4000, Station Main; fan.zhang@drdc-rddc.gc.ca.

Experimental studies in tubes larger than 10-cm-diam have been conducted since the 1980s. Tulis and Selman [11] conducted aluminum–air experiments in a 15.2-cm-diam tube but with a short length of 5.5 m, using 3 g of condensed explosive for initiation. It was found that detonation can only be achieved in flake aluminum with a surface area to mass ratio of 3–4 m^2/g, equivalent to spherical particles of diameter less than 1 μm. The detonation velocity observed in this facility was unstable, fluctuating between 1350 and 1640 m/s with a deficit of 10–30%. Later, Borisov et al. [17] reported more consistent aluminum–air detonation velocities between 1700–1800 m/s in a 12.2-cm-diam tube for 1 μm atomized particles and 1 μm thick flakes. A strong direct initiation of detonation technique was employed due to the short tube length of 4.2 m, thus it was unclear whether the detonation wave observed was still influenced by the initiation. Gardner et al. [12] used a large tube 60 cm in diameter by 42 m in length and recorded the transition with a violent onset to detonation in a coal dust–air mixture. At the end of the tube, the transient velocity of the combustion wave reached 2850 m/s and a peak pressure of 80 atm was measured. However, the tube, with a length-diameter ratio of 70, was still too short to record a self-sustained detonation wave. Conclusive evidence of the existence of a self-sustained detonation wave in solid particle-oxidizing gas flow has been established since the late 1980s through detailed observation of the transverse wave structure using a 14 cm and a 30-cm-diam tube with a length-diameter ratio larger than 120 [13–16,19]. DDT in a tube with layered grain particles was investigated by Li et al. [22] in a 30-cm-diam and 70-m-long horizontal air-filled tube.

Whereas a large transverse wave spacing is inherent to detonations in micrometric solid particle–air flow, reactive particles added to a detonable gas mixture can cause a variety of detonation modes as a result of the interaction between the gas reaction and the additional physical processes involved in the mass, momentum, and heat transfer between the two phases. Fast deflagration of particles in gas detonation flow may enhance gas detonation and DDT, and has been referred to as "hybrid detonation" and "hybrid DDT" [23–33]. In 1982, Veyssiere et al. [23,24] reported for the first time the observation of a detonation wave composed of a double-shock in a lean reactive gas mixture with aluminum particles at concentrations ranging 15–80 g/m^3. The test was conducted in a 6-m-long apparatus consisting of a 4.5-m-long by 6.9-cm-diam circular tube connected to a 5.3-cm-square tube. Independently, in the same time period, Afanasieva et al. [25] theoretically postulated the existence of "double-shock" detonation in multiphase media. Khasainov and Veyssiere [26] employed a two-phase (Zeldovich, von Neumann and Döring) ZND model and showed that a "steady" double-shock detonation structure can exist, in which the two fronts are stabilized by the generalized Chapman–Jouguet (C–J) condition for the particle–gas mixture. Their further analysis explored the multiplicity of steady solutions for given initial conditions due to nonmonotonic behavior of the heat release process [27]. Wolinski et al. [28] studied hybrid detonations in oats particles suspended in methane–air mixtures and observed that the addition of oats particles may promote methane–air detonation, and that a secondary compression wave appeared due to the late particle combustion. Recent experiments have provided more conclusive evidence on the self-sustained propagation of double-shock detonation and explored other hybrid detonation modes [29–32]. It has been shown that the double-shock detonation waves can be considered as the weak detonation solutions supported by the particle reaction. DDT in hybrid mixtures with large concentrations of aluminum particles near a tube end wall was also reported to result in a peak pressure of more than twice that produced in the same gas system alone [33]. This was attributed to the reverberating shock compression and initiation dynamics in a dense combustible particle layer. The variety and complexity of hybrid detonation waves and their propagation mechanisms have yet to be understood fully and remain an active area of current detonation research.

The present paper mainly reviews the selected works in which the author has been involved and addresses the physical phenomena of detonation observed in dilute, reactive solid particle–gas flow and the discrepancies between experiments and theories. Selected topics include multiphase detonation theory, transition to detonation, detonation structure, dynamic parameters, quasi detonation, and hybrid detonation. Regarding the propulsion engine applications, most of the discussion is limited to researches under tube confinement and relevant comments are included in the Concluding Remarks.

Multiphase Detonation Theory

The equilibrium C–J detonation theory assumes a detonation wave to be a strong discontinuity within which the chemical reaction has ended and produces a final equilibrium detonation products state at a frozen sonic locus with respect to the detonation wave. A unique steady solution to the one-dimensional conservation equations across the discontinuity can be found to correspond to the minimum detonation velocity solution where the Rayleigh line is tangent to the final equilibrium Hugoniot curve. The C–J steady solution has been remarkably successful to predict detonation velocity in uniform gas, liquid, and solid matter for conditions well within the detonation limits, given a reasonable equation of state for the detonation products. The detonation pressure, temperature, and flow velocity obtained from the C–J theory can be considered as the mean values at a mean frozen sonic locus averaged over the cross section perpendicular to the direction of propagation. It has been experimentally difficult, however, to determine the sonic locus where the averaging can be taken behind the shock front [34–37] because, in reality, detonation waves have a three-dimensional structure. The success of the C–J theory lies in the simplicity of assuming a strong discontinuity without the need to consider the details of chemical nonequilibrium processes and the detonation wave structure. This assumption, however, prevents one from gaining insights into detonation initiation and propagation mechanisms responsible for predicting detonation velocity deficit, failure limits, as well as other dynamic parameters.

Apart from the chemical nonequilibrium process, detonation of a solid particulate two-phase mixture comprises other nonequilibrium processes of mass, momentum, and energy transfer between the two phases due to finite sizes of solid particles. A complete or final equilibrium state includes all chemical, mechanical (pressure and particle velocity), and thermal (temperature) equilibrium between the phases. In general, the nonequilibrium momentum and heat transfer depend on the physical properties of the particles and do not have the same relaxation length scales as that of the mass transfer or chemical nonequilibrium processes. Because the C–J theory assumes a unique final equilibrium detonation products state at the sonic locus, it cannot predict the detonation velocity precisely for finite-sized particulate mixtures with large interphase momentum and heat transfer length scales.

Figure 1 illustrates the predictability of the C–J theory by comparing the theoretical predictions from the Cheetah code [38] with the experimental results obtained in aluminum particles-RDX ($C_3H_6N_6O_6$) mixtures at a constant initial mixture density of 1.66 g/m^3 [39]. RDX was chosen due to its oxygen deficiency. For sufficiently small particles (e.g., 0.1 μm), an increase in aluminum mass fraction results in a decrease in detonation velocity. The experimental detonation velocities are in agreement with the theoretical prediction, regardless of the reactive or chemically frozen nature of the particles. This fact clearly indicates the significance of the momentum and heat transferred to the particles toward the mixture equilibrium state as the flow approaches the sonic locus, and that the momentum and heat transferred are responsible for the velocity deficit with respect to pure RDX detonation. In contrast, for sufficiently large particles (e.g., 5 μm), the experimental velocity is much higher than the final equilibrium prediction and close to that of pure RDX, thus suggesting a nearly frozen transfer of momentum and heat between the two phases within the detonation zone. The experimental detonation velocity is therefore a strong function of particle size and ranges between the final equilibrium value and the frozen limit.

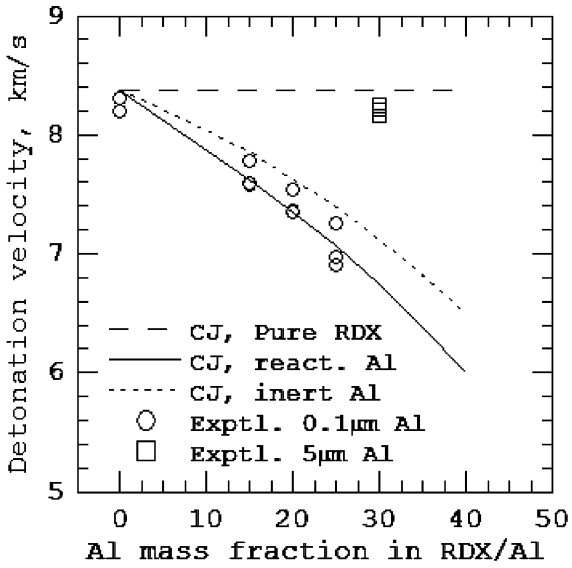

Fig. 1 Comparison of experimental detonation velocities with the equilibrium C–J theory for aluminum particle-RDX mixtures.

The ZND detonation model in uniform matter developed by Zeldovich, von Neumann and Döring assumes a detonation wave structure that consists of a leading shock front followed by a continuous reaction zone. The leading shock front adiabatically compresses a material to an autoignition temperature to initiate chemical reaction while the expansion of high-pressure reacting gasses in turn provides work to sustain the propagation of the shock front. A unique steady solution is obtained by integrating the one-dimensional ordinary differential conservation equations along the reaction progress path to the C–J sonic locus, where the Rayleigh line is tangent to the final equilibrium Hugoniot curve. To calculate detonation velocity deficits and detonation limits, Zeldovich and others further proposed a quasi-one-dimensional model in which the source terms are introduced in the conservation equations to consider lateral boundary effects such as friction and heat loss to the tube wall or expansion into the surroundings [40,41]. Because of the presence of loss source terms competing with exothermic reactions, the flow may become sonic before the final chemical equilibrium, such that the ideal C–J sonic condition is no longer valid. An alternative, referred to as the "generalized C–J condition," was introduced as a mathematical saddle point on which the exothermic heat release rate equals the energy loss rate at the gaseous frozen sonic locus with respect to the shock front. For a reactive system with nonmonotonic heat release behavior, Kuznetsov [42] demonstrated that the steady ZND solution may not be unique and multiple detonation solutions are possible for given initial conditions. Theoretically, the one-dimensional ZND structure may be oscillating [43–50] whereas real detonation waves have an unstable three-dimensional structure. Hence, the one-dimensional detonation wave structure (the profiles of pressure, temperature, and flow velocity along the reaction path) obtained from the steady ZND model may be regarded as a mean structure averaged over the cross section perpendicular to the direction of propagation, and over an oscillating period in the propagation direction.

For solid particle-fluid mixtures, strictly speaking, a steady solution cannot be achieved a priori without integration along the reaction path to determine the mechanical and thermal partial-equilibrium between the two phases. Hence, a two-phase ZND model has been introduced with a generalized C–J condition as a rear boundary condition, where the net heat release rate resulting from the chemical reactions and interphase nonequilibrium mass, momentum, and heat transfer approaches zero at the gaseous frozen sonic locus [26,27,51–61]. Two-phase, steady, one-dimensional governing equations can be derived from the control volume analysis of the continuum theory. These include mass, momentum, and energy conservation equations for each phase, continuity equations for species and conservation equations for solid particle numbers, with a volume fraction saturation constraint (i.e., the sum of the volume fractions of all phases equals unity). The governing equations must satisfy the conservation laws of the mixture when summing the conservation equations for the fluid and solid phase. In the governing equations, the fluid and the solid particles are treated as two separate continua and their interactions are described using source terms for the rate of mass, momentum, and energy transfer. Solid particle agglomeration or breakup is controlled through a source term for the rate of particle number change. When the solid particle flow is granular or extremely dense ($\phi_p \geq 0.1$), a dynamic compaction equation must also be employed where a source term is introduced to describe the rate of solid volume compaction [53–55,60]. The latter is caused by mechanical nonequilibrium between the internal stresses and the forces exerted by neighboring particles and the interpore fluid. If the reaction zone is large, the loss due to the tube wall or other lateral boundary conditions must also be included and modeled by the source terms for the rate of the momentum and heat exchange with the lateral boundaries. Various forms of source term functions can be found in [26,27,51–61]. Whereas in a rigorous multiphase continuum theory the source terms must follow constraints imposed by the conservation laws and the entropy inequality of the mixture, they are modeled on the basis of fundamental physical rules and empirical correlation. Therefore, appropriate choice of the source term functions for a particular flow topology is crucial for the reliability of the solution.

From the governing equations in the coordinate frame, with respect to the leading shock front propagating at velocity D, a system of ordinary differential equations can be formed in which the change of the fluid velocity u_1 along the propagation distance x is given by

$$\frac{du_1}{dx} = \Psi/\eta \tag{1}$$

where

$$\eta = 1 - u_1^2/c_{f1}^2 \tag{2}$$

is a sonic parameter of the flow with respect to the gaseous frozen sound speed c_{f1}. The quantity Ψ represents the "thermicity", a measure of the rate of transformation from net energy release from all nonequilibrium processes to molecular and bulk translational energy. A "generalized multiphase C–J condition" serves as the rear boundary condition at the gaseous frozen sonic point imbedded in the reaction zone by finding the common zeros of the thermicity Ψ and the sonic parameter η:

$$\Psi = 0 \quad \text{at} \quad \eta = 0 \tag{3}$$

The detailed expression of the thermicity depends on the nonequilibrium processes and equations of state. To elucidate the physical meaning of the net heat release rate, an analytical expression is given next for a simple system comprising a perfect gas with single exothermic (heat $q_1 > 0$), irreversible gaseous reaction (rate $w_1 > 0$), and a negligible volume fraction of solid particles ($\phi_p = 0$, $p_p = 0$) with exothermic particle combustion (heat $q_p > 0$, *rate of mass transfer* $J_p > 0$) and constant particle number

$$\Psi = \frac{\gamma - 1}{\rho_1 c_{f1}^2}\left\{q_1 w_1 + \sum_{p=2}^{N}(q_p + c_p T_p)J_p - \sum_{p=2}^{N}\left[\left(u_p - \frac{\gamma u_1}{\gamma - 1}\right)f_p + Q_p + \frac{(u_1 - u_p)}{2}\left(u_p - \frac{(\gamma + 1)u_1}{\gamma - 1}\right)J_p\right] + \left(\frac{\gamma u_1}{\gamma - 1} - D\right)f_W + Q_W\right\} \tag{4}$$

The first term on the right-hand side of (4) describes the energy release rate of the gas-phase reaction. The second term (with source term J_p) represents the rate of energy release in the gas due to particle evaporation and reaction that can take place in vapor phase or on heterogeneous surfaces. The third term (in square brackets)

corresponds to the rate of gas energy change caused by the nonequilibrium flow velocity and temperature between the two phases. The rate of momentum transfer f_p and the rate of energy transfer Q_p have the same sign as the phase velocity difference $u_1 - u_p$ and phase temperature difference $T_1 - T_p$, respectively. The last two terms (with the W subscript) represent the rate of gas energy change due to momentum and heat transfer to lateral boundaries. The value of f_W or Q_W is negative if the exchange results in a loss to the lateral boundaries. For finite-sized particle–gas flow, the nonequilibrium momentum and heat transfer between the two phases described in the third term can result in an energy loss rate competing with exothermic reaction rates of the first and second terms at the gaseous frozen sonic locus, thus providing an intrinsic mechanism satisfying the generalized C–J condition (3). In this case, the lateral boundary source terms f_W and Q_W will quantitatively change solution values, but are not necessary in satisfying condition (3) and the steady solution. To clearly elucidate the intrinsic mechanism for the multiphase detonation, all examples in this paper do not include lateral boundary source terms.

The ordinary differential equation system deduced from the governing equations, the equations of state for the particles and gas phase, together with the generalized C–J condition (3), form the closure of the mathematical description of the two-phase ZND model, given the source terms for the exchange between the two phases and to the lateral boundaries. Thus, under the initial conditions of the postshock state, a steady solution can be obtained for the propagation velocity and reaction zone structure of the detonation wave in a reactive particle-oxidizing fluid system, in an inert particle-reactive fluid system, or in a reactive particle-reactive fluid system. It is well known in the gas detonation theory that a steady ZND solution may be unstable and the stability of a steady solution can be studied by a linear stability analysis [43,46,47] or through direct numerical simulations of the unsteady conservation equations [44,45,48–50]. As the activation energy in a single-step Arrhenius rate law, or the induction-to-reaction length ratio using a multistep reaction scheme, decreases below the value for the stability limit, the steady solution can also be obtained by the longtime asymptotic solution of the one-dimensional unsteady conservation equations. This asymptotic solution approach is also valid for the multiphase detonation [59].

The steady ZND detonation structure in a dilute, reactive particle-oxidizing gas system consists of a shock front followed by an induction and reaction zone successively and is terminated at the gaseous frozen sonic locus where the generalized C–J condition (3) is satisfied. In the induction zone, whereas a drag force results in a momentum loss for the gas due to the momentum transferred to the particles, the drag compression continuously increases the gas pressure and temperature. Significant heat release of the particles takes place after the induction and the resultant gas expansion causes the pressure to decrease when the flow moves toward the sonic locus. The expansion of the high-pressure gasses provides the work to sustain the propagation of the shock front which, in turn, supports the momentum and heat transfer between the two phases behind the shock front and the ignition of particles. Hence, unlike the ZND structure for uniform fluid detonation where the shock front pressure (i.e., the von Neumann spike) corresponds to the maximum pressure, the maximum pressure for a reactive particles-oxidizing fluid detonation wave is located behind the shock front at a point at which the combustion expansion balances the drag compression. It is also noticeable that, unlike uniform fluid detonation, the equivalence ratio of the particle-fluid mixture behind the shock front does not remain the same as the initial value ahead of the shock front. The velocity relaxation time lag, in which the particle is accelerated toward the fluid velocity before burning, results in a shift of the equivalence ratio from the initial value toward a leaner value. Korobeinikov [62] indicated that a high particle concentration layer may form farther downstream under conditions of an appropriate velocity relaxation time lag behind the shock. The particle concentration in this so called ρ-layer could be several times higher than the initial value. In such conditions, the equivalence ratio immediately behind the shock front could be even smaller. The late combustion of the ρ-layer and its influence on the detonation flow remain a subject of current research for experiments and unsteady numerical modeling.

The steady ZND detonation structure in a dilute, inert particle-reactive gas system is analogous to a frictional detonation [63,64], in which the frictional force is replaced by a drag force determining the momentum transfer from the gas to the particles. Figure 2 shows an example in a mixture of stoichiometric acetylene–air modeled by a single-step Arrhenius rate law and 10 μm inert aluminum particles with a 500 g/m^3 concentration [59]. The drag force influences the wave structure in two aspects. Whereas it causes a shock velocity deficit with respect to the gas C–J detonation and therefore a drop in postshock gas pressure and temperature, the drag compression in the gas reaction zone gradually amplifies gas pressure and temperature. For the current particle size and concentration, the velocity and temperature relaxation length scales of the particle flow are two orders larger than the gas reaction zone length. Thus, the drag compression is more than compensated by the gaseous combustion expansion, so that the pressure monotonically decreases from the shock front to the sonic locus. Whereas the combustion expansion causes gas density to decrease from the postshock value, particle concentration is gradually increased from the initial value, due to the velocity relaxation time lag in which the drag force drives the particles. The competition of the gas-phase chemical energy release with the momentum and heat transfer to the solid particles results in a detonation velocity $D = 1800$ m/s that has a mild deficit of -3.2% relative to the C–J velocity of the gas detonation ($D_{\text{Gas CJ}} = 1860$ m/s), but an increase of 10% with respect to the complete or final equilibrium C–J velocity ($D_{\text{CJ}} = 1632$ m/s).

The generalized C–J locus determined by (3) is a mathematical saddle point, after which the subsonic flow relative to the shock front can become supersonic as it reaches the weak detonation branch of the final equilibrium Hugoniot curve. Two important conditions must be met for a steady weak detonation solution as follows:

1) The necessary conditions are a) within the reaction zone, there is at least one gaseous frozen sonic point imbedded at which the generalized C–J condition is satisfied; and b) the final equilibrium Hugoniot is not the upper bound of all partial-equilibrium Hugoniot curves.

2) The uniqueness of a steady weak detonation solution depends on the flow or boundary conditions behind the generalized C–J point.

A simple illustrative example is the well known detonation wave in a perfect gas with an irreversible exothermic reaction followed by a secondary irreversible endothermic reaction (heat releases $q_a > 0$, $q_b < 0$, $|q_a| > |q_b|$) [65]. It has a saddle point featured with the generalized C–J condition (3) imbedded in the reaction zone due to

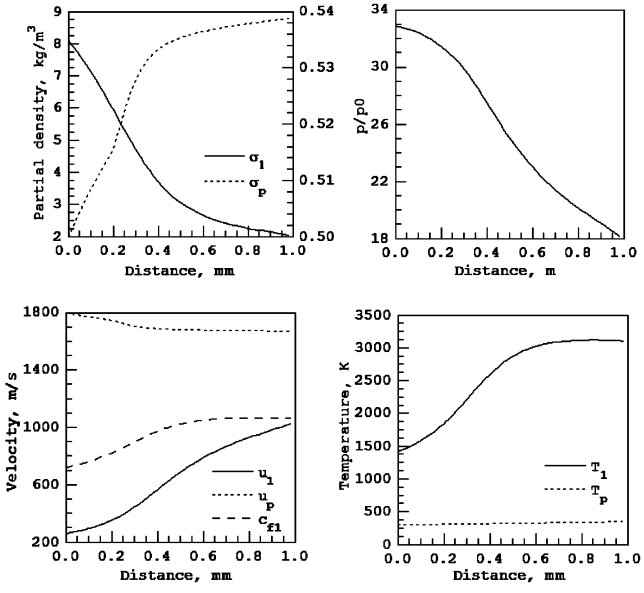

Fig. 2 ZND detonation structure in a mixture of stoichiometric acetylene–air and inert aluminum particles.

the endothermic reaction rate competing with the exothermic reaction rate. A steady solution can be obtained by integration of the ZND model from the postshock state downstream to satisfy the generalized C–J condition at which the Rayleigh line is tangent to a partial-equilibrium Hugoniot curve. This partial-equilibrium Hugoniot corresponds to the highest attainable heat release of the system, $Q_{\max} = q_a + q_b[1 - \exp(q_a/q_b)]$, that is larger than the heat release $Q_f = q_a + q_b$ in the final equilibrium Hugoniot. Therefore, the solution satisfies the necessary conditions for a weak detonation and it is then possible to continue the integration from the saddle point downstream, as the flow smoothly transits from subsonic to supersonic until it meets the final equilibrium Hugoniot curve. The detonation velocity D_m corresponding to the Rayleigh line tangent to the $Q_{\max}$-Hugoniot is greater than the final equilibrium detonation velocity D_{CJ}. Depending on the rear flow or boundary conditions, the solution can either return to a strong detonation point along the D_m-Rayleigh line or down to the weak detonation point where the flow is supersonic. The solution is incomplete without taking into account the second condition stated in the preceding section. A variety of weak detonation solutions can be obtained when the detonation wave is followed by a piston of specified constant velocity by adjusting the piston velocity [65].

For a solid particle–gas flow, a partial-equilibrium state also includes that of mass, momentum, and energy transfer processes between the two phases. In fact, detonation in an inert particle-reactive gas system as shown in Fig. 2 satisfies the necessary conditions for a weak detonation. It has a saddle point imbedded in the reaction zone as depicted by the generalized C–J criterion (3). Secondly, the final equilibrium Hugoniot lies below some partial-equilibrium Hugoniot curves because the final equilibrium detonation velocity is smaller than that shown in Fig. 2. After the gaseous sonic locus, the solid particle velocity and temperature will further equilibrate with that of the gas phase toward the final equilibrium Hugoniot as the flow becomes supersonic with respect to the leading shock front.

Detonation in a dilute reactive particle-reactive gas system is analogous to the detonation wave for two irreversible reactions with the second reaction endothermic, followed by a piston of specified constant velocity. The momentum and heat loss from the gas to the particles provides a mechanism to satisfy the necessary conditions for a weak detonation (e.g., Fig. 2), whereas various weak detonation solutions can be realized by controlling the late particle energy release to match the rear flow condition behind the saddle point. The energy release rate of particles represented by the second term in the thermicity (4), denoted as $q'_p J_p$, is a characteristic parameter to specify a possible solution. The delay time and the magnitude of $q'_p J_p$ can be adjusted through the particle material, size, or concentration, as well as gaseous detonation parameters or products compositions. Consequently, a set of solutions can be obtained as displayed in Fig. 3 using the numerical solution of the unsteady conservation equations [30–32]. Note that the solutions discussed next are only some examples important in practice due to their enhancement to the gas detonation impulse loading. Different perspectives on the complexity and multiplicity of the hybrid detonation solutions can also be found in [27]. It is also noticeable that the calculation time for the asymptotic steady solutions shown in Fig. 3 is not long enough and therefore the solutions only serve for the quantitative description of physical phenomena. The supersonic or subsonic flow terminologies used in the following discussions are with respect to the leading shock front.

1) If $q'_p J_p$ rises early and significantly, particle reaction can produce a compression wave in the gas reaction zone to increase detonation velocity and pressure [Fig. 3a (2 μm Al at 300 g/m^3)]. The entire subsonic reaction zone is substantially extended due to particle combustion and a steady solution is reached when the generalized C–J condition (3) is satisfied at the gaseous frozen sonic locus. There exists a minimum in the pressure profile within the reaction zone when the net heat release reaches a local maximum at thermicity $\Psi = 0$ before the sonic locus. This solution is referred to as "single-front detonation" by Veyssiere and Khasainov [27], but was termed a "strong hybrid solution" [31,32] in the sense that particle combustion within the reaction zone overdrives the gas detonation. This terminology came from the analogy with detonation in an exothermic–endothermic two-reaction gas followed by a piston moving faster than the flow velocity of the strong detonation point. However, unlike the usual overdriven detonation, where the entire flow is subsonic with respect to the leading shock front, a strong hybrid detonation will not be disturbed by the supersonic rear flow behind the sonic locus. A strong hybrid detonation wave usually occurs for reactive particles suspended in a lean reactive gas mixture,

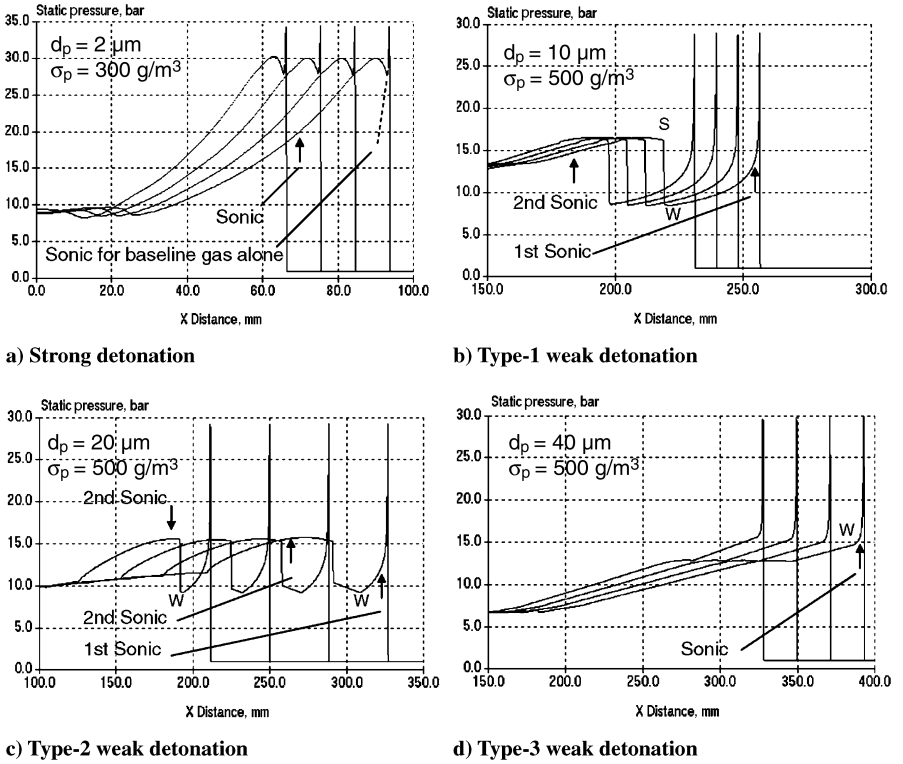

Fig. 3 Hybrid detonation solutions in a mixture of lean acetylene–air and aluminum particles.

where the rate of particle energy release into gas overcomes the loss rate due to the momentum and heat transferred from gas to particles within the gas reaction zone. In a system of fine reactive particles suspended in a rich reactive gas mixture, the strong hybrid detonation is unlikely to take place due to the prevailing rate of momentum and heat loss that leads to a detonation velocity deficit and instability.

2) When $q'_p J_p$ is delayed and reduced to enable particle reaction behind the gas reaction zone, particles behave as though inert within the gas reaction zone and the necessary conditions for a steady weak detonation can be satisfied, where a generalized C–J point appears for the first time [Fig. 3b (10 μm Al at 500 g/m^3)]. In the supersonic gas flow behind the first sonic point, heat release from the particles would cause a continuous decrease in gas flow velocity to subsonic levels, and an increase in gas pressure. This, however, will not match the downstream unsteady supersonic flow required by the rear boundary condition, and instead will result in thermal choking. Consequently, a second shock wave is necessary to adjust the gas flow behind the gas reaction zone from supersonic to subsonic. The flow, with the heat release from the particles, is then able to expand toward the second sonic locus, where the generalized C–J condition is satisfied a second time to match the downstream unsteady supersonic flow. Thus, a double-shock solution can be achieved that consists of the steady gas reaction zone followed by a secondary shock. The $q'_p J_p$-induced second shock wave corresponds to a postshock subsonic state S and a preshock supersonic point W behind the steady gas reaction zone. If the Rayleigh line SW coincides with that for the leading front, the second shock moves with the same velocity as the leading front. This solution is referred to as the type-1 double-shock weak solution, analogous to the double-shock solution in the two-reaction gas followed by a piston velocity equal to the flow velocity of the strong detonation point.

3) When $q'_p J_p$ decreases, the velocity of the $q'_p J_p$-induced second shock wave is reduced. The shock therefore recedes from the supersonic end state W of the steady gas reaction zone to produce an ever-widening region of supersonic flow between state W and itself [Fig. 3c (20 μm Al at 500 g/m^3)]. As $q'_p J_p$ further decreases, the strength of the secondary shock decreases and recedes more rapidly. This solution is called the type-2 double-shock weak solution, in analogy to the solution in the two-reaction gas followed by a piston with velocity between that of the strong detonation point and the weak detonation point. Unlike the weak detonation in the two-reaction gas followed by a piston, the ever-widening region of the supersonic flow is unsteady. The initial particle combustion increases the pressure and decreases the flow velocity upstream of the secondary shock. Furthermore, the particle reaction zone length between the second shock and the second sonic locus increases continuously as the shock recedes. Rigorously speaking, a steady solution does not exist after the end point W of the steady gas reaction zone.

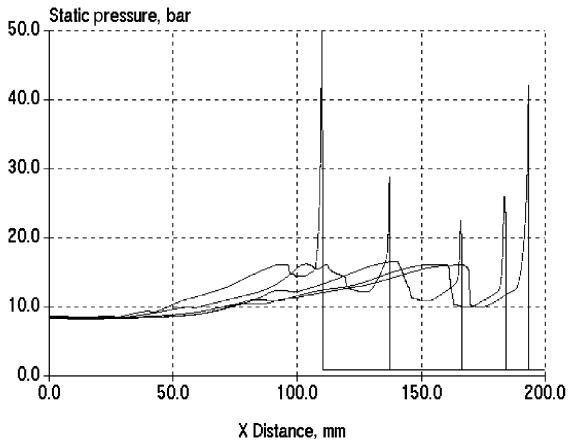

Fig. 4 Numerical simulation of unsteady weak hybrid detonation with a transient secondary pressure wave.

4) As $q'_p J_p$ is further delayed and reduced, the supersonic end point W of the steady gas reaction zone is connected to the supersonic rear flow imbedded with a weak compression wave caused by the particle combustion [Fig. 3d (40 μm Al at 500 g/m^3)]. The solution is regarded as the type-3 hybrid weak solution, analogous to the solution in the two-reaction gas followed by a piston velocity equal to the flow velocity of the weak detonation point. Whereas the detonation front propagates steadily and satisfies the generalized C–J condition (3) at the gaseous frozen sonic locus, the particle-reacting rear flow is unsteady and subject to the rear boundary condition. The particles become chemically inert as $q'_p J_p$ is reduced to approach a null value.

The one-dimensional multiphase ZND model possesses unique features in detonation stability [31,59,66–68]. Whereas in a reactive particle-reactive fluid system, reaction of the particles within the fluid reaction zone stabilize the detonation (e.g., Fig. 3a), the momentum and heat transferred from the fluid to the particles within the fluid reaction zone destabilize the detonation for any solid particle-reactive fluid systems. This momentum and heat transfer causes a velocity deficit with respect to the C–J detonation velocity of the pure fluid. The magnitude of the velocity deficit depends on the ratio of the velocity or temperature relaxation length scale of solid particles L_p to the fluid ZND detonation zone length L_{1r} that is,

$$\frac{L_p}{L_{1r}} \sim \frac{d_p^n \rho_p^m}{\sigma_p^t L_{1r}} \tag{5}$$

where $n, m, t > 0$ [59]. Thus, increasing particle concentration σ_p, or decreasing particle diameter d_p and material density ρ_p, will increase the detonation velocity deficit and instability. One can use numerical solutions of the unsteady governing equations to examine the validity of a steady ZND solution. For instance, for detonation in an inert particle-reactive gas system displayed in Fig. 2, L_p was two orders of magnitude larger than L_{1r}. Consequently, a small velocity deficit of -3.2% resulted and the longtime asymptotic unsteady solution appeared in accordance with the steady ZND solution. When $L_p/L_r \sim 1$ or less, rapid momentum and heat transfer within the gas reaction zone resulted in a large velocity deficit and caused the detonation wave to fail. For a range of intermediate values of L_p/L_{1r}, the detonation executed an unsteady oscillatory behavior and the oscillation irregularity increased as L_p/L_{1r} decreased, indicating that the ZND multiphase model is unstable for a range of intermediate velocity deficits. The generalized multiphase C–J condition failed in unstable detonation waves and the detonation limits predicted by the unsteady solution appeared to be more restricted than that obtained from the steady solution [59,63]. Caution must therefore be taken when using the steady solution to predict the detonation limits. For detonation in a reactive particle-reactive gas system, Fig. 4 illustrates a numerical simulation for a 1000 g/m^3 concentration of 10 μm aluminum particles suspended in a lean acetylene–air system [31]. In comparison with the steady double-shock detonation wave shown in Fig. 3b, an increase in particle concentration results in an increase in velocity deficit from -3% to -8%, thus causing the detonation wave to propagate in an unstable oscillatory mode. Whereas the particles still burn behind the gas reaction zone, the energy release from the particle combustion is coupled with the unsteady rear flow of the gas detonation. Consequently, a transient pressure wave is generated behind the detonation front. In an oscillatory cycle, the pressure wave has an acceleration phase followed by a deceleration phase. The acceleration phase leads to the formation of a shock wave before the deceleration phase commences. Analysis and numerical simulations on the instability of a detonation wave in a reactive aluminum particle-oxidizing gas system can be found in [69–73].

Finally, noting that the source term functions are modeled according to fundamental physical rules and empirical correlations, the reliability and predictability of the two-phase continuum theory are strongly determined by the choice of source term functions for a particular flow topology, as well as the equations of state and chemical reaction kinetics [39,53–55,60,74]. For instance, in handling the momentum transfer in detonation of solid particles

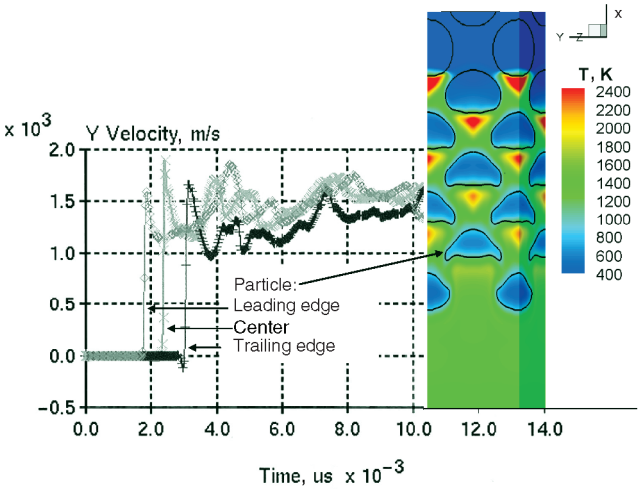

Fig. 5 Numerical velocity histories for the leading particle in a 1 g/cm³ liquid–aluminum particle system subjected to a 101.3 kbar shock.

suspended in low-density gas flow (e.g., Fig. 2), the shock interaction time in which the shock front crosses a particle is several orders of magnitude smaller than the velocity relaxation time related to the drag. Thus, a solid particle is assumed to remain stationary as the shock front crosses it [75]. In contrast, for detonation in high-density gas flow or condensed matter containing light metal particles, the shock interaction time can be comparable to the drag-induced velocity relaxation time due to a significant increase in initial material density ratio of fluid to particles. Mesoscale modeling showed that the postshock velocity for aluminum particles achieved 70–80% of the shocked flow velocity of a liquid (Fig. 5) and the momentum transferred during the shock interaction time was a strong function of the initial fluid-to-particle material density ratio and the volume fraction of solid particles [39,74]. Hence, caution must be taken in employing appropriate source term functions with respect to the two-phase flow topology involved. The source term functions and chemical reaction kinetics of solid particles remain an essential challenge confronted by the current two-phase continuum detonation theory and numerical modeling. Associated problems will be further discussed in this paper.

Transition to Detonation

Detonation of solid particles reviewed in this paper includes cornstarch, anthraquinone, and aluminum [13–15,19,20,30–32,76,77]. The cornstarch $(C_6H_{10}O_5)_n$ had an approximately spherical shape with a mean size of 10μm, and the anthraquinone $(C_{14}H_8O_2)$ was in strip form with an average size of $22 \times 6 \times 6$ μm^3. Various aluminum particles were investigated, including spherical particles ranging from 100 nm to 22 μm and 1 μm thick flakes with an average area of 36×36 μm^2. These three types of particles were different in their sensitivity to constant volume explosion. The sensitivity increases from lowest to highest in cornstarch, anthraquinone, and 1 μm characteristically sized aluminum [4]. Experimental results reviewed in this paper were mainly conducted at the Shock Wave Laboratory of RWTH Aachen, and Defence Research and Development Canada at Suffield, in three round tubes equipped with a particle dispersion system. Their inner diameters and test section lengths were 8 cm with a 10 m length, 14 cm with a 17.4 m length, and 30 cm with a 37 m length. All three tubes possessed a length-diameter ratio larger than 120.

A deflagration-to-detonation transition process in reactive solid particles suspended in oxidizing gas or air flow in tubes can be divided into a slow reacting compression stage and a fast reacting shock stage when relatively weak initiation is employed. Figures 6–8 show the typical DDT pressure records and flame front trajectory using 13 pressure transducers and 13 ion gauges along the propagation distance of the 30-cm-diam tube filled with cornstarch–air or flaked aluminum–air mixtures at 1 bar initial pressure [19]. Early in the reacting compression stage, the compression wave is slowly amplified. The compression wave amplification coupled with the chemical energy release by the flame can be clearly recognized through the flame front trajectory crossing the backside of the compression waves. For the lean aluminum–air mixture shown in Fig. 8, the reacting compression stage becomes a multiple compression one, in which the second compression wave is amplified at $50 < x/d < 105$ behind the precursor shock front that was developed from the first compression wave. The multiple compression stage was also observed in lean cornstarch–oxygen mixtures [77]. As a result of the reacting compression stage, a critical shock wave forms with a Mach number between 3.1 and 3.5 (at $x/d \sim 95$ and 105 in Figs. 6 and 8 for less sensitive mixtures and $x/d \sim 35$ in Fig. 7 for more sensitive mixtures). Near the formation of the critical shock wave, a rapid increase in flame velocity is observed as shown in Fig. 9. This might indicate that the critical shock wave would be defined not only by a Mach number but also by the temperature gradients behind the shock front. An understanding of the underlying mechanism of detailed turbulent combustion of particles in the reacting compression stage would require further researches with advanced diagnostics.

The formation of the critical shock marks the beginning of the reacting shock stage in which the flame accelerates rapidly due to close coupling with the shock amplification, as observed in homogeneous gas DDT [78,79]. Within a propagation distance of the reacting shock of about 20 tube diameters in Figs. 6 and 8, and less than 10 tube diameters in Fig. 7, an abrupt onset of overdriven detonation takes place and brings the flame velocity to its maximum (Fig. 9). If normalized with the characteristic detonation cell size, to be reviewed later, the propagation distance of the reacting shock, which begins from the formation of the critical shock and ends at the onset of the maximum overdriven detonation, amounts to about six detonation cell sizes for all three mixtures. Whereas the onset of the overdriven detonation for less sensitive mixtures, such as cornstarch–air and lean aluminum–air, is clearly accompanied by a retonation wave propagating backward (Figs. 6 and 8), the retonation

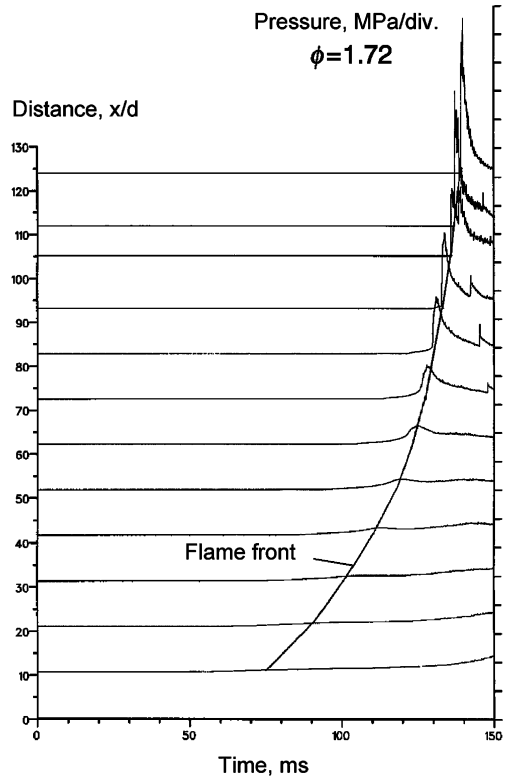

Fig. 6 DDT in a 400 g/m³, 10 μm cornstarch–air mixture using four 300 J pyrotechnical igniters.

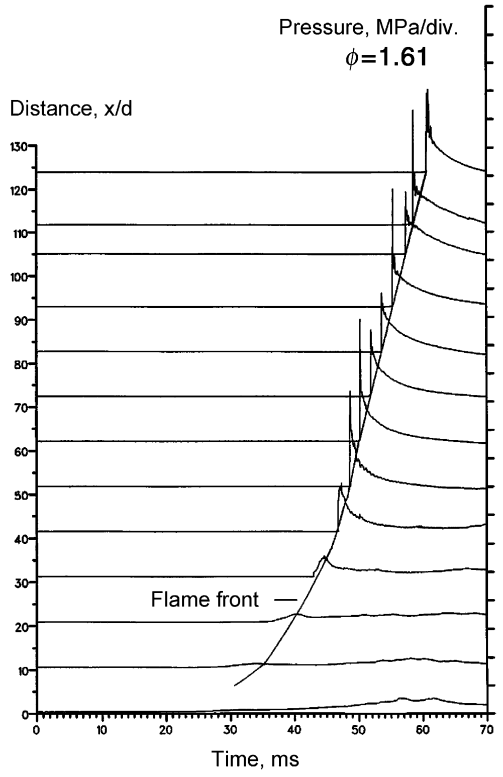

Fig. 7 DDT in a 500 g/m^3, 36 × 36 × 1 μm flaked aluminum–air mixture using a 300 J pyrotechnical igniter.

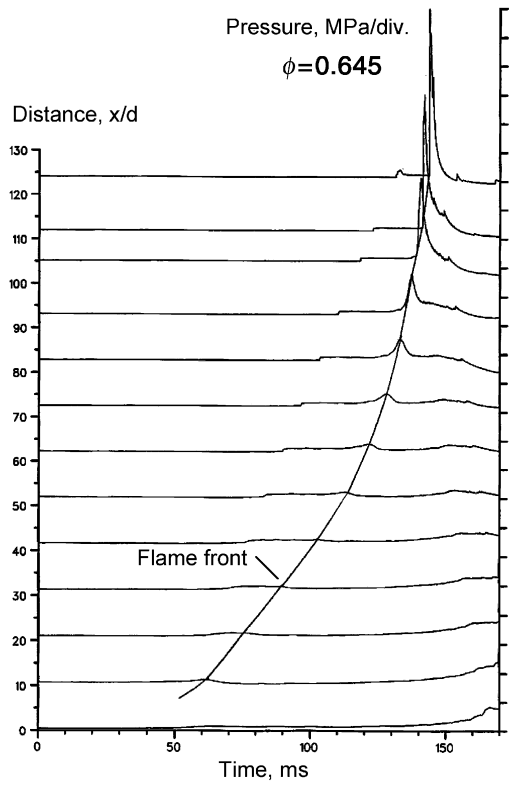

Fig. 8 DDT in a 200 g/m^3, 36 × 36 × 1 μm flaked aluminum–air mixture and a 300 J pyrotechnical igniter.

wave in rich aluminum–air is rather weak, as shown in Fig. 7. After its maximum, the overdriven detonation wave begins to relax toward a stable transverse wave detonation mode.

The stable detonation structure is characterized in the shock wave front and the oscillation frequency recorded in multiple pressure profiles distributed on a tube circumference. Figure 10 displays a single-head spinning wave in the 30 cm tube for the rich cornstarch–air mixture that was used in the DDT experiment of Fig. 6. The single transverse wave head can be recognized between the profiles numbered 1 and 8. The single-head spinning mode was observed over a wide range of fuel equivalence ratios between 0.7 and 3 at 1 bar initial pressure. For anthraquinone–air mixtures, the single-head spinning mode was obtained in the 14 cm tube over a range of fuel equivalence ratios between 1.7 and 2.2 at 1 bar initial pressure [76].

Figure 11 shows a detonation wave with multiple transverse wave heads in the 30 cm tube for the rich flaked aluminum–air mixture with DDT displayed in Fig. 7. Four transverse wave heads can be recognized on one tube circumference at traces 1, 3, 5, and 6. This, together with a pressure oscillation period of about 200 μs, indicates at least two detonation cells around the tube circumference with a mean cell size approximately equal 0.45 m. Borisov et al. [17] observed spinning detonation in a 12.2-cm-diam tube for 1 μm atomized aluminum particles and 10 × 10 × 1 μm^3 flakes. Because of a short tube length of 4.2 m (i.e., a length-diameter ratio of 34), they employed a strong direct initiation of detonation. Therefore, it is possible that the observed spinning detonation wave had not reached the self-sustained mode at that tube end. Unlike the organic particles, the pressure oscillations behind the aluminum detonation front displayed in Fig. 11 manifest themselves in small amplitudes and vanish within a short time.

The single-head spinning detonation has been accepted as the lowest stable, self-sustained detonation mode in a tube for homogenous gas mixtures. The corresponding tube diameter is therefore referred to as the minimum tube diameter $d_{\min}$, a necessary boundary condition for the transition to and propagation of a stable detonation [80]. The minimum tube diameter for detonation in solid particle–gas flow is of at least one order of magnitude greater than that in most detonable gas mixtures.

The insensitivity of aluminum–air detonation was further demonstrated through DDT in Fig. 12 where the initial particle diameter was reduced to 0.1 μm and the initial pressure was 1 atm using a 6 kJ detonator [20]. A multiple compression DDT process was observed in the 8-cm-diam tube and transition to a single-head spinning detonation occurred near the end of the tube. The propagation distance of the reacting shock equals about 20 tube diameters or six characteristic detonation cell sizes again. This result on nanometric particles clearly indicates that the insensitivity of aluminum–air detonation is attributed not only to heterogeneous transport processes, but also to a high-melting-point oxide layer that passivates the surface of each particle.

For the solid particle–air detonation waves with spinning structures or transverse wave structures, the experimental detonation velocities are summarized in Fig. 13 for anthraquinone in a 14-cm-diam tube [76], in Fig. 14 for cornstarch in a 30-cm-diam tube [19], and in Fig. 15 for aluminum in a 12-cm-diam tube [17], 30-cm-diam tube [19], as well as an 8-cm-diam tube [20]. These experimental velocities are in agreement with the values computed from the equilibrium C–J theory within about 10% deviations (in Fig. 15, the

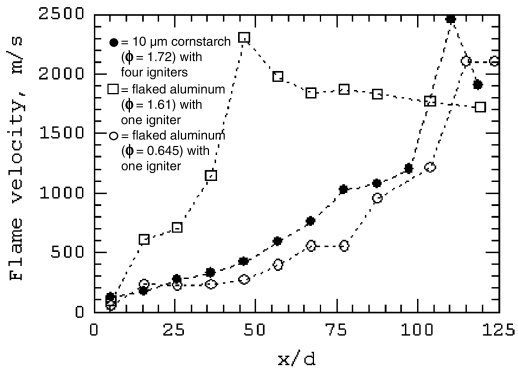

Fig. 9 Flame velocities of particle–air mixtures using 300 J pyrotechnical igniters.

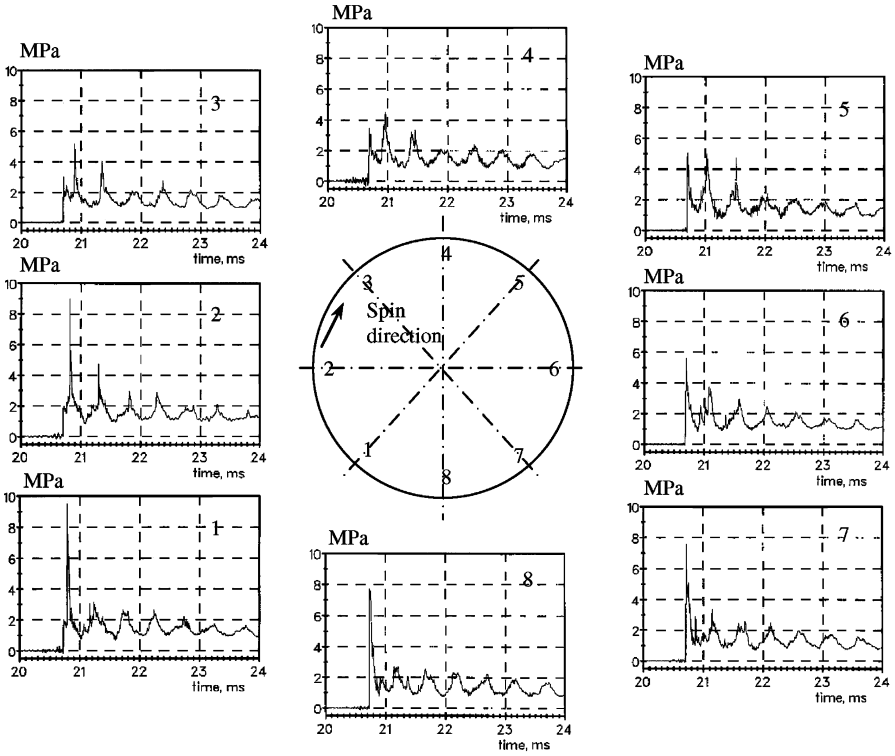

Fig. 10 Pressure profiles in a 400 g/m^3, 10 μm cornstarch–air mixture ($\phi = 1.72$).

low velocity values for 0.1 μm Al at less than 1 atm and 2 μm Al will be discussed in the section on quasi detonation). Noting that the 0.1μm aluminum particles were passivated with an oxide coating to a mass fraction of about 10%, its detonation performance was expected to be less energetic than that of pure aluminum used in the calculation. Agreement with equilibrium C–J theory indicates that the transverse-wave-structured detonation velocity is mainly determined by the energetics. The C–J detonation velocities display a shift toward the lean side and the reasons are twofold: 1) a shift in postshock equivalence ratio from the initial toward a leaner value due to a particle velocity relaxation time lag before particle combustion, and 2) a shift in real particle concentration from the nominal value indicated on the horizontal coordinate toward a leaner value due to sedimentation and adhesion of particles to the tube wall during experimental dispersal. As the mixtures become richer for cornstarch and aluminum, the calculated C–J velocity drops, however, the

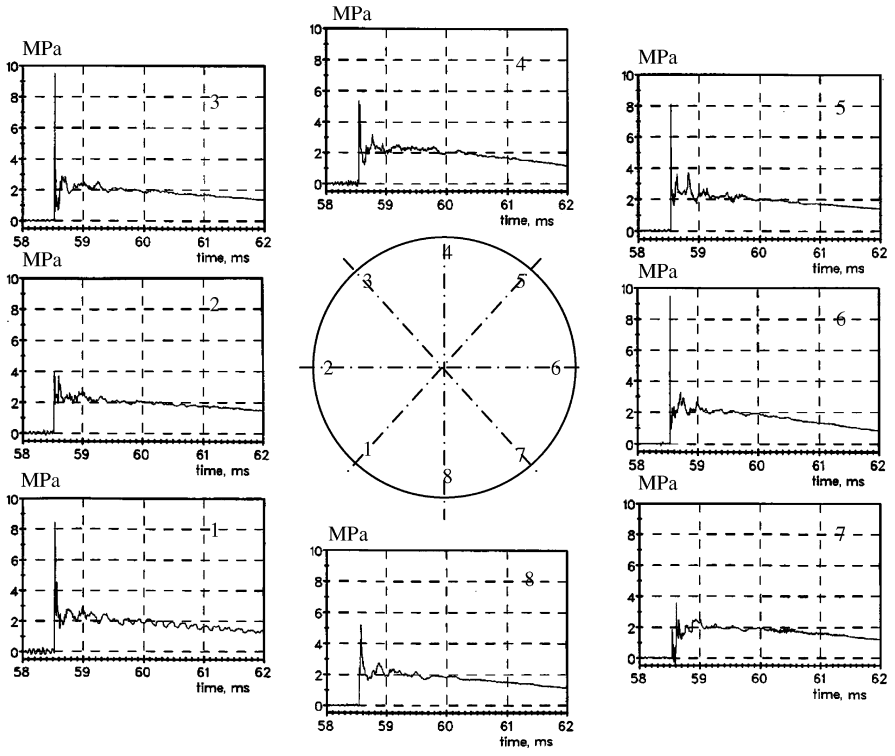

Fig. 11 Pressure profiles in a 500 g/m^3, 36 × 36 × 1 μm flaked aluminum–air mixture ($\phi = 1.61$).

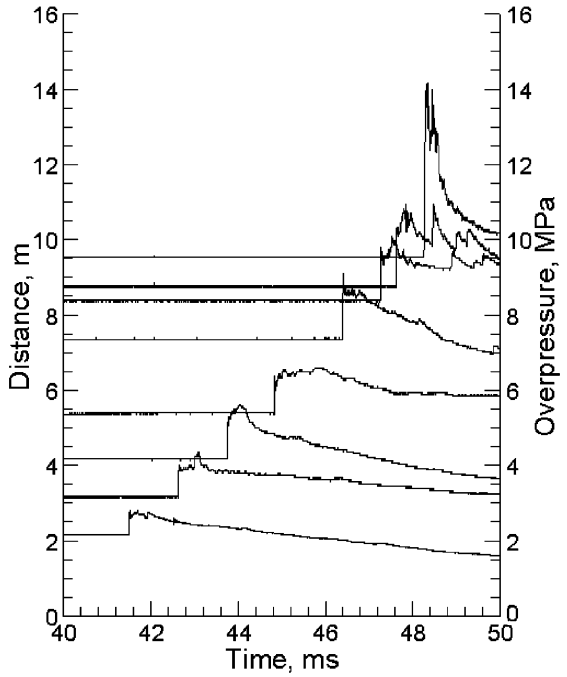

Fig. 12 DDT in a 400 g/m^3, 0.1 μm spherical aluminum–air mixture ($\phi = 1.29$).

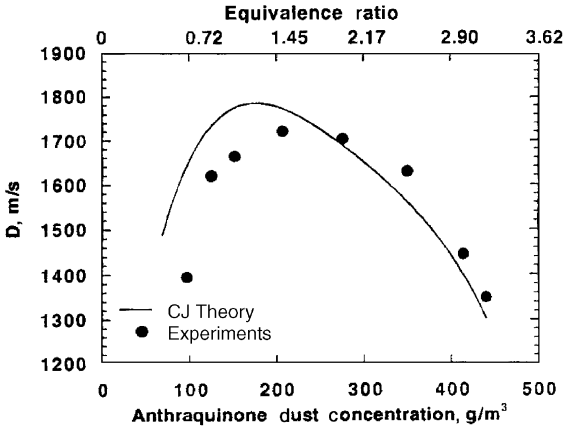

Fig. 13 Detonation velocities in 22 × 6 × 6 μm anthraquinone particle–air mixtures at 1.15 bar initial pressure.

experimental results show only a slight decrease or a "plateau" extending from the peak values. This unique plateau feature has also been observed over a range of rich particle concentrations in particle-oxygen mixtures [15]. It is probably due to the time lag of momentum and heat transfer from gaseous products to unburned particles and their agglomerates in the hot products. Hence, the equilibrium C–J theory may not be applicable to mixtures with very rich particle concentrations.

Apart from particle sedimentation and adhesion that cause experimental difficulties in achieving a uniformly dispersed two-phase mixture as assumed in the equilibrium C–J theory, there are two inherent reasons responsible for detonation velocity deviations as discussed in the section on multiphase detonation theory. First, contrary to the fundamental postulate of the equilibrium C–J theory, detonations in reactive particle–gas mixtures are essentially nonideal where momentum, heat, and chemical equilibrium between the two phases may not be achieved at the gaseous frozen sonic plane. Second, momentum and heat loss induced by lateral boundary layer effects behind the shock front increases within a large reaction zone corresponding to the transverse wave spacing.

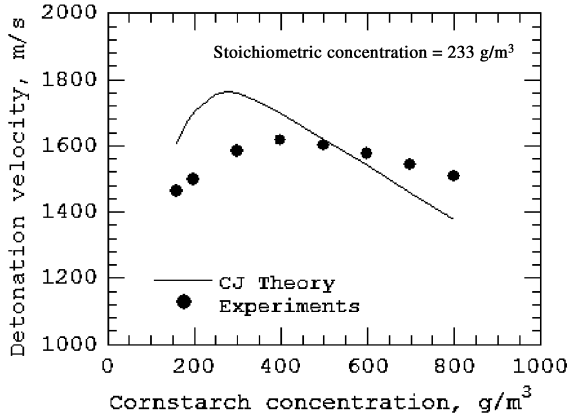

Fig. 14 Detonation velocities in 10 μm cornstarch–air mixtures at 1 bar initial pressure.

Experimental determination of the C–J detonation pressure is more difficult than the detonation velocity in relatively insensitive particle–gas mixtures because the large transverse wave spacing of the detonation front provides various pressures along the three-dimensional shock front and a number of oscillations to the pressure profiles behind the front (see Figs. 10 and 11). Rather than attempting to interpret the C–J pressure from an oscillatory pressure record, the experimental "peaks" and "valleys" were averaged over a period behind the front and the resultant median was comparable to the equilibrium C–J pressures [15].

Detonation Structure

For homogeneous gasses, the single-head spinning and cellular detonation waves have been considered as the stable transverse wave detonation modes with a triple point configuration as the basic feature [80–91]. There are, however, significant differences between the propagation mechanisms for the two kinds of detonation waves. For the single-head spinning detonation, the coupling of the chemical reaction and acoustic vibration in tubes results in a helical propagation of the triple point configuration, moving with a velocity along a track angle. Hence, the main geometry of the wave front remains despite the perturbations that can take place in higher orders. On the other hand, in a cellular detonation wave collisions between triple points are necessary for a self-sustained propagation.

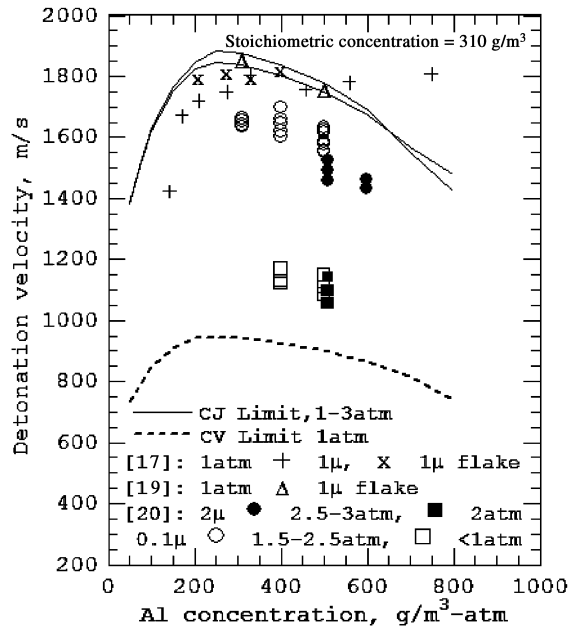

Fig. 15 Detonation and quasi-detonation velocities in aluminum–air mixtures in various diameter tubes.

Therefore, the frontal geometry and propagation of the triple points become transient. The single-head spinning and cellular detonation waves have also been observed in heterogeneous particle–gas mixtures [13–15,19,20].

Figure 16 displays a single-head spinning structure at the detonation front around the 14 cm tube on circumference in a 0.5 bar stoichiometric cornstarch–oxygen mixture [13]. This structure was observed through the use of a large number of pressure-ion double front gauges distributed on the tube circumference at several axial cross sections. The frontal structure manifests itself primarily in a transverse shock wave that propagates into the induction zone behind the incident shock and produces a traveling triple point configuration at the front. The transverse wave velocity observed on the periphery is approximately equal to the axial propagation velocity, thus resulting in a spinning track angle $\alpha = 45$ deg at the front around the tube wall.

The interior structure of the single-head spinning detonation in the same mixture was also measured by using 25 pressure transducers at the center and in three inner circles within one cross section of the 14 cm tube [13]. The leading shock surface showed an interior spinning structure whose surface curvature was gradually reduced towards the center. The unison of the oscillation phase in radial lines observed in the pressure profiles yielded a constant angular velocity $\omega = 25.55 \times 10^3$ rad/s. Therefore, an ideal single-head spinning detonation wave possessed two propagation velocities at the detonation front, that is, the axial propagation velocity D and the angular velocity ω. The incident flow entered the leading shock front under the spinning track angle $\alpha = \tan^{-1} r\omega/D$ which had a maximum at the tube wall and approached zero on the axis. These experimental observations were also verified by the solution of the Navier–Stokes equations and the continuity equation [13]. The detailed interior structure, and that immediately behind the leading shock front, have not been resolved even for homogenous gas mixtures. A spatially continuous, high resolution diagnostic method, such as laser-optical visualization technology has been recently applied to explore the structure of the gaseous detonation front by combination of laser schlieren images showing the density field, and planar laser induced fluorescence (PLIF) images to illustrate slices of OH concentration field behind the leading shock front [92,93].

A two-head spinning or a single-cell detonation wave was also recorded in the 14 cm tube with the same diagnostic method for a rich cornstarch–oxygen mixture [14]. The collision of two triple points led to an overdriven wave followed by a transient decoupling between the shock and chemical reaction. Because the two triple point configurations moved in the opposite direction on the circumference, successive collisions made the continual reignition to

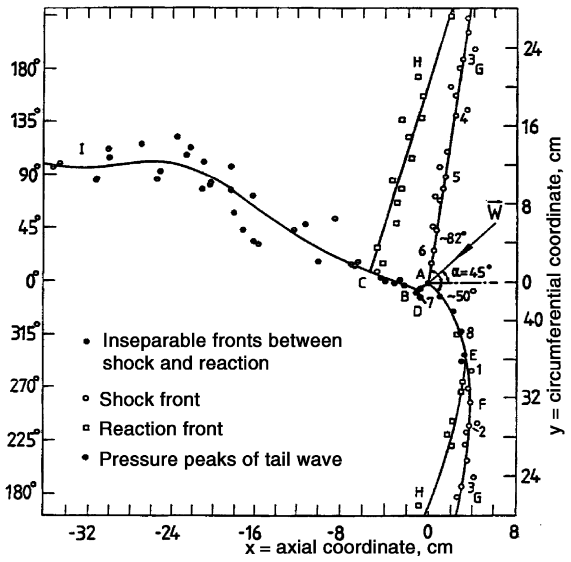

Fig. 16 Spinning detonation front structure in a 554 g/m^3, 10 μm cornstarch–oxygen mixture ($\phi = 1$).

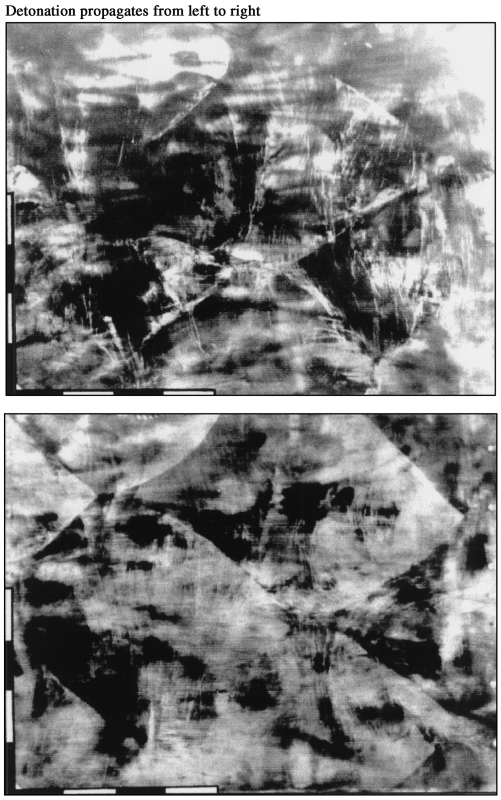

Fig. 17 Cellular detonation structure from smoke foil records in a 440 g/m^3, 10 μ cornstarch–oxygen mixture.

sustain the detonation wave possible. The triple point trajectories formed a single cell with a cell width of $\lambda \sim \pi d$. The experiments produced a transverse wave velocity of $C \approx 0.62D$ and a mean track angle of $\alpha = \tan^{-1}(C/D) \approx 32$ deg, where D was the mean axial propagation velocity. The two-head detonation wave cannot exist without boundary confinement.

Figure 17 shows smoke foil records of a cellular detonation structure observed from two experiments in the 30 cm tube for a $\phi = 0.8$ cornstarch–oxygen mixture at 0.5 bar initial pressure [19,94]. The soot photographs display more than one and one-half cells in the 0.8 m wide foil. The average cell size and length measured from the soot photographs are $\lambda = 0.50$ m and $L = 0.77$ m. This results in a mean track angle of the triple point trajectory of $\alpha = \tan^{-1}(\lambda/L) \approx 33$ deg and an average transverse wave velocity of $C = (\tan\alpha)D \approx 0.65D$.

Discussion on Dynamic Parameters

In the theory of gas detonation, the correlation by Zeldovich et al. [95] links the minimum tube diameter for propagation of a stable, self-sustained detonation wave to the cell width of the cellular detonation by

$$d_{\min} \approx \lambda/\pi \tag{6}$$

This also defined a characteristic cell size λ for the single-head spinning detonation because it has been considered to be the lowest stable, self-sustained detonation mode [80]. Numerous gas detonation experiments have proven that relation (6) is appropriate for fuel–air detonation, but may underpredict the minimum tube diameter for fuel–oxygen mixtures [96,97]. For the cornstarch–oxygen mixtures as reviewed in the previous section, the measured cell size, $\lambda = 0.50$ m at the equivalence ratio $\phi = 0.8$ (Fig. 17), is consistent with the characteristic cell size of the single-head spinning mode, $\lambda \sim \pi d = 0.44$ m at $\phi = 1$ (Fig. 16). Although more experiments are required to draw a firm conclusion, this consistency suggests that relation (6) is applicable to the heterogeneous detonation of reactive particles in air but also in oxygen. This could

be attributed to detonation in reactive particle–gas flow possesses a large transverse wave spacing imbedded with numerous distributed hot or flame spots induced by the particles. Therefore, the detonation is relatively insensitive to small disturbances in the boundary layer on the tube wall. Hence, relation (6) has been applied to the single-head spinning detonation waves, reviewed in the section on transition to detonation, to evaluate characteristic cell sizes for various mixtures. The resulting characteristic cell sizes for the three types of reactive particles suspended in air or oxygen at various equivalence ratios are listed in Table 1. The evaluated cell sizes for the particle–air detonation waves range typically between 0.25 and 1 m at 1 atm initial pressure, thus being at least one order larger than that for the detonation in most gas–air mixtures.

In the DDT processes shown in Figs. 6–9, pyrotechnical igniters with an initiation energy of 1.2 kJ were used for cornstarch–air and 0.3 kJ for flaked aluminum–air. Hence, an initiation energy of10^2–10^3 J can be considered a "weak" initiation for reactive particle–air DDT that leads to slow deflagration during the initial stage. This fact indicates that an initiation energy for reactive particle–air DDT is at least three orders greater than that for gaseous DDT using weak initiation. The requirement of a three-order-higher initiation energy was also found when comparing dust explosions to gas explosions in closed vessels [4]. Considering the one-order-larger cell size in the particle–gas detonations compared with gas detonations, it is reasonable to scale the initiation energy to the cube of the characteristic detonation cell size for reactive particle-oxidizing gas mixtures, a power scaling rule well demonstrated for gaseous detonations [95,98–100]. Lacking direct experimental data, the correlation of the critical energy for direct initiation of gaseous detonation [99]

$$E_{\mathrm{cr}} = \frac{2197}{16}\pi I \rho_0 D^2 \lambda^3 \tag{7}$$

has been assumed to estimate the critical energy and critical charge mass for direct initiation of unconfined reactive particle-oxidizing gas detonation, based on the characteristic cell sizes and the experimental steady detonation velocities. The estimated values are listed in Table 1, from which the critical initiation energy and charge mass typically range between 20–200 MJ and 5–50 kg, respectively, for unconfined aluminum particle–air detonation at 1 atm initial pressure. This estimate only serves as a reference; the accurate values must be obtained from direct measurements performed in large-scale experiments which are the current subjects of research. For a number of experiments in tubes, a hydrogen–oxygen or acetylene–oxygen detonation driver was often used to initiate the reactive particle–gas detonation directly. A method to evaluate the initiation energy for a detonation driver can be found in [77].

For organic particles with a high volatile content, detonation sensitivity is increased with increasing initial pressure p_0. In the same cornstarch–air mixtures, although the single-head spinning detonation was found in the 30 cm tube, it was observed in the 14 cm tube only when the initial pressure was raised to between 2 and 2.5 bar [77]. These results suggest that the high volatile organic particle–gas detonation approximately follows the scaling rule of gaseous detonation [101–103], in which the detonation cell size is inversely proportional to initial pressure:

$$\lambda \sim p_0^{-m}, \qquad m = O(1) \tag{8}$$

Correlation (8), together with relation (6), links the minimum tube diameter $d_{\min}$ with the detonation cell size at an initial pressure p_0. The approximately inverse proportionality of λ on p_0 arises from the approximate linearity of p_0 on the oxygen concentration above certain lower initial pressure limits. Hence, $m = O(1)$ indicates a reaction mechanism strongly dependent on gas-phase kinetics for these organic particle–gas detonation waves.

Aluminum particles possess a high melting-point oxide coating that must be melted or cracked open before aluminum can react. In quiescent atmospheric or low-speed flow conditions, the ignition of aluminum particles had a threshold temperature near the oxide melting point of 2300 K. Above the threshold temperature, classical fuel droplet diffusion theory applies for the combustion of relatively large particles according to the earlier experimental observations [104,105]. The fuel droplet diffusion theory states that the particle burning time is proportional to a power of its initial diameter, $t_b \sim d_0^n$ where $n = 2$. It assumes infinite kinetics and is essentially independent of pressure and temperature. For the combustion of aluminum particles smaller than 30 μm in atmospheric conditions, the diffusion theory could lead to underprediction of the burning rate [106–108]. In typical solid rocket motor conditions (10^1–10^2 atm and above 2300 K), it has been found that the burning rate of aluminum particles is greater than that in 1 atm air, thus resulting in a smaller power n between 1 and 2 and pressure dependence [109–113]. The power $n < 2$ implies the effect of finite gas-phase kinetics and possibly convective flow effects [114]. Because the burning aluminum mass flux is inversely proportional to particle radius (yielding $t_b \sim d_0^2$) in the diffusional transport and independent of particle radius (yielding $t_b \sim d_0$) in the kinetic process, the diffusional transport rates approach infinity as particle diameter approaches zero, whereas kinetic process rates do not increase with decreasing particle size. Therefore, at sufficiently small particle diameters, the use of the d^2-law becomes incorrect and the particle combustion must become kinetics-limited.

As for the ignition of aluminum particles in quiescent or low-speed flow conditions, the measured ignition delay time was proportional to a power of particle diameter, $t_I \sim d_{p0}^2$, following the convective heat law for a diameter range of 2–30 μm at 6–11 bar pressures in excess of a threshold temperature of 2100 K [115]. Foelsche et al. [111] reported a weak pressure dependence of $t_I \sim p_0^{-0.6}$ at a higher pressure range up to 38 bar for 22 and 53 μm particles. On the other hand, aluminum particles were ignited much below the oxide melting point in the shock tube experiments. Borisov et al. [116] observed an ignition temperature of about 1400 K for 15–20 μm aluminum particles after a reflected shock, and it would be expected to be even lower for 1–2 μm particles. A temperature of 1000–1400 K results in a vapor pressure of 10^{-5}–10^{-1} Pa only, thus indicating the improbability of diffusion-limited evaporation ignition in shocked conditions. Experiments were also conducted to ignite particles by a shock wave immediately followed with a detonation expansion flow, using a hydrogen–oxygen detonation driver connected with an air-filled driven section in which particles were initially located 50 mm

Table 1 Dynamic parameters for detonation of solid particles in oxygen or air[a]

Material	Equivalence ratio	One-head spin tube diameter $d_{\min}$, m	Detonation cell size λ, m	Direct initiation energy E_{cr}, MJ	Direct initiation charge M_{cr}, kg TNT
10 μm cornstarch–air	0.7–3	0.3	0.96	950–1070	196–220
10 μm cornstarch–O_2	0.45–1.5	0.14	0.44	148–163	30–33
10 μm cornstarch–O_2	2.5–4.5	<0.14 (2-head spin)	0.44	148–163	30–33
10 μm cornstarch–O_2	0.8–1	0.14 @ 0.5 atm	0.44–0.5 @ 0.5 atm	87	18
Anthraquinone–air, 6 μm strips	1.7–2.2	0.14	0.44	112–125	23–26
0.1 μm Al–air	1–1.6	0.08	0.25	22–23	4.5–4.7
Flaked/atomized 1 μm Al–air	1–2	0.12–0.14	0.38–0.45	92–128	19–26
Flaked Al–air	0.65	0.3	0.96	1290	265
Atomized 2 μm Al–air	1.6	0.08 @ 2.5 atm	0.51–0.62	150–270	30–56

[a]The initial pressure is 1 atm if not specified.

from the driver section [117]. The observed ignition delay time tended toward $t_I \sim d_{p0}$ for a wide aluminum particle diameter range of 2–110 μm, further suggesting possible influences of the kinetics-limited ignition.

Because aluminum–air detonation only occurs for a particle characteristic size less than a few micrometers and the particles ignite and burn between the shocked (>40p_0 and 1500–2000 K) and subsequent detonation (>20p_0 and 3000–4000 K) conditions, one would expect that finite kinetics could affect the aluminum reaction. Recent experiments showed that an increase in initial pressure increases the detonation sensitivity and reduces the DDT distance for 0.1 μm aluminum particle–air mixtures in the 8 cm tube using the same initiation charge mass (see Fig. 12 for $p_0 = 1$ atm and Fig. 18 for $p_0 = 1.5$ atm) [20]. Note that a nominal particle concentration is introduced in Fig. 18 with a unit of grams per cubic meter and per atm to keep the same equivalence ratio in air for various initial pressures. By increasing the aluminum particle size to 2 μm, transition to single-head spinning detonation was observed only when the initial pressure was increased to 2.5 atm, whereas at 2 atm and below no transition to detonation occurred within the tube length, as displayed in Fig. 19. These experimental observations clearly indicate the pressure-dependence of initiation, transition, and propagation of the aluminum–air detonation, thus suggesting a role of finite kinetics in the aluminum ignition and reaction mechanism under detonation conditions.

Taking the preceding discussions into account, correlations for the ignition delay and burning time of fine aluminum particles can be proposed as $t_I \sim d_0^n/p_0^m$ and $t_B \sim d_0^{n'}/p_0^{m'}$, where n, $n' \leq 2$, m, $m' \leq 1$ under detonation conditions. Assuming that the minimum tube diameter for aluminum particle–gas detonation $d_{\min}$ or the detonation cell size λ is proportional to the reaction timest_I and t_B, one obtains

$$\pi d_{\min} \sim \lambda \sim d_0^n/p_0^m \quad \text{with} \quad n \leq 2,\ m \leq 1 \tag{9}$$

Relation (9) is an analogy to that of gaseous detonation where the detonation cell size is scaled to the induction time. [95,98–100]. Applying this relation to the experimental data in [20] results in $m = 0.77$–1 and $n = 1$–1.3 for the 2 μm aluminum–air detonation. Thus, it indicates a dependence on initial pressure and gas-phase kinetics. It is noticeable that this analysis was limited to a rather global and qualitative approach to elucidate the importance of limited kinetics on the aluminum reaction mechanism in detonation. Ultimate understanding and solution rely on the development of detailed kinetic schemes of aluminum reaction under conditions of aluminum–air deflagration and detonation. The influence of high-momentum flow immediately behind the shock on the physical properties of the particles and the aluminum reaction must also be quantitatively determined [116–122].

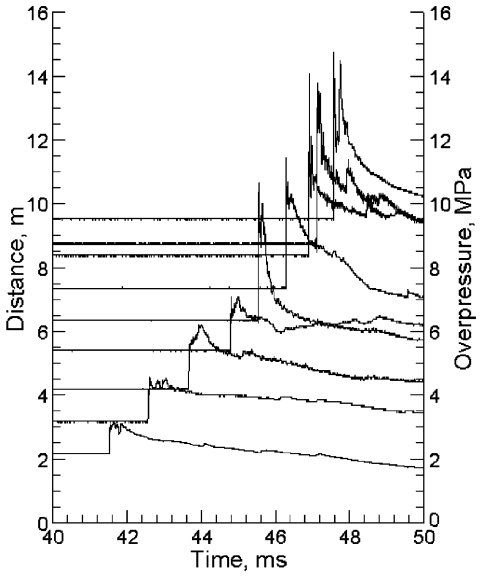

Fig. 18 DDT in a 400 g/m^3-atm, 0.1 μ aluminum–air mixture ($\phi = 1.29$) at 1.5 atm.

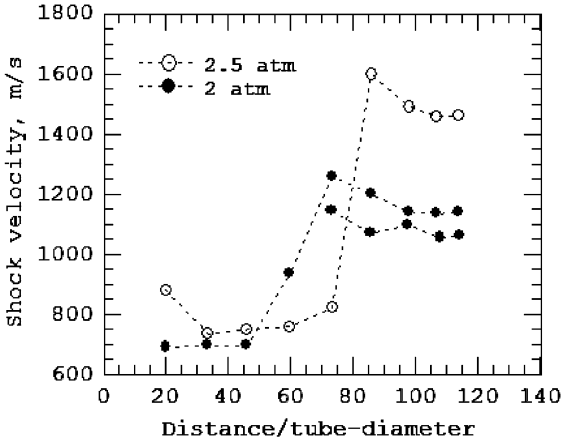

Fig. 19 Transition from deflagration to quasi detonation or detonation in 500 g/m^3-atm, 2 μ aluminum–air mixtures ($\phi = 1.61$).

Quasi Detonation

In homogeneous gas mixtures, it is well established that detonation waves propagate at less than the equilibrium C–J detonation velocity as the tube diameter is reduced to around the detonation cell size, due to boundary layer effects and losses to the tube wall [96,97,123–128]. Moen et al. [96,97] indicated that mixtures with irregular cellular structures are influenced less by the confining tube walls than the regular-cell mixtures. Whereas fuel–air detonation waves with irregular structures exhibit velocity deficits within 3% of the theoretical C–J value and fail at $d \leq \lambda/\pi$, detonations in fuel–oxygen and argon-diluted mixtures with fairly regular structures show larger velocity deficits above 10% and fail in a larger tube at $d \leq (1.3\text{–}2)\lambda/\pi$. In general, detonation failure in gaseous mixtures is associated with the disappearance of the transverse wave structure.

Unlike homogeneous gaseous detonations, a shock-induced supersonic combustion wave can propagate quasi-steadily in tubes much smaller than the detonation cell size in a reactive particle-oxidizing gas flow [10,20,77], due to distributed particle-induced explosion or hot spots that make the combustion less sensitive to the disturbance originating in the boundary layer on the tube wall. The observed shock-induced combustion waves were characterized by a shock velocity much less than the equilibrium C–J detonation value, and a relatively smooth pressure profile behind the shock front without fully developed, self-organized transverse wave structure. Such a shock-induced combustion wave may be referred to as "heterogeneous quasi detonation." Figure 19 shows an evolution to a quasi-detonation wave by two experiments in the 8 cm tube filled with a 2 μm spherical aluminum–air mixture at 2 atm initial pressure. After propagating through 70 tube diameters at low velocities, the wave rapidly accelerates to a shock velocity of 1080–1140 m/s and propagates quasi-steadily to the tube end thereafter. Thus, the quasi-detonation wave propagates at $d \sim (0.4\text{–}0.5)\lambda/\pi$. The wave has a velocity deficit nearly 40% with respect to the theoretical C–J value, and displays compression waves behind the shock front without periodically oscillating inherent transverse wave structure (Fig. 20). In fact, this shock speed is close to the critical Mach number that could lead to DDT. Behind the shock front, local explosions take place that can be identified by the high compression peaks with subsequent retonation waves propagating backward. However, the wave is not able to further accelerate to a transverse wave mode detonation because of the small tube confining the transverse wave development. Note that the test section length of 120 tube diameters may still be insufficient to conclude whether or not the quasi-detonation wave can maintain its steadiness. Quasi detonation was also found in rich cornstarch–air

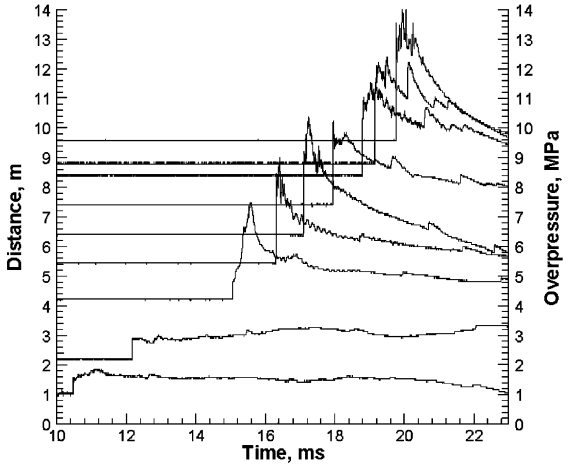

Fig. 20 Transition from deflagration to quasi detonation in a 500 g/m^3-atm, 2 μ aluminum mixture at 1 atm ($\phi = 1.61$).

mixtures [77] in the 14 cm tube ($d \sim 0.46\lambda/\pi$) and in cornstarch–oxygen mixtures [10] in a 5.3-cm-square tube ($d \sim 0.4\lambda/\pi$).

A quasi-detonation wave fails when the distributed particle explosions are suppressed by the momentum and heat transferred from gas to particles as well as the expansion and turbulent quenching originating in the boundary layer on the small tube wall. One may predict quasi-detonation limits using the steady multiphase ZND model or, more restrictively, by the unsteady solution as discussed in the section on multiphase detonation theory. In the one-dimensional theory, the gas flow velocity with respect to the tube wall v_1 is positive but decreased with the distance behind the shock front due to the gas-phase momentum losses to the particles and to the tube wall. Hence, a lower limit can be proposed in which the gas flow velocity with respect to the tube wall has been decreased toward zero at the gaseous frozen sonic plane [129]. Any dust quasi-detonation wave cannot propagate below this absolute limit because the entire flow would become subsonic with respect to the shock front and the generalized C–J condition (3) would be no longer satisfied. Applying $v_1 = 0$ at the sonic plane to the same two-phase conservation equations of mass, momentum, and energy used for the ZND model as well as the generalized C–J condition (3), one obtains at the gas-phase frozen sonic plane

$$\rho_{\rm cr} = \sigma_{1,0} + \sigma_{p,0} \tag{10}$$

$$e_{\rm cr} = \frac{(\sigma_{1,0}e_{1,0} + \sigma_{p,0}e_{p,0})}{\sigma_{1,0} + \sigma_{p,0}} + \frac{\int_0^{x_{\rm cr}} Q_W \, {\rm d}x}{(\sigma_{1,0} + \sigma_{p,0})D_{\rm cr}} \tag{11}$$

$$D_{\rm cr} = c_{f1,{\rm cr}} \tag{12}$$

where the subscript "0" denotes the initial state in front of the shock and the subscript "cr" represents the state at the gaseous frozen sonic plane. Equations (10–12) mean that the wave structure begins with a shock front propagating at a critical velocity $D_{\rm CR}$ and ends with a constant volume (CV) combustion boundary at the gaseous frozen sonic plane. Note that for simplicity, the lower limit model (10–12) was obtained by further assuming that at the sonic plane, the solid particle velocity with respect to the tube wall approaches zero. Thus, it may not be applicable to large-sized particulate mixtures. Under the adiabatic assumption $Q_W = 0$, the absolute lower limit becomes independent of the nonequilibrium processes and the equilibrium CV combustion calculation with (10–12) results in pressure $p_{1,{\rm cr}}$, temperature $T_{1,{\rm cr}}$, and frozen gas sound speed $c_{1f,{\rm cr}}$ equal to the critical shock velocity $D_{\rm cr}$.

The experimental propagation velocities of detonations and quasi detonations are bounded between the equilibrium C–J detonation values and the equilibrium CV explosion lower limits. This is shown in Figs. 15 and 21, respectively, for aluminum–air and cornstarch–oxygen mixtures in various sizes of tubes under different particle dispersion and initiation conditions. In Fig. 21, data from [13] used a 14-cm-diam tube and data from [10] used a 5.3-cm-diam tube. Except for the unique plateau feature for rich particle concentrations, a maximum velocity deficit of 10% generally holds for the detonation with transverse wave structure. In the case of the quasi-detonation waves, however, measured shock velocities indicate a deficit as much as beyond 40% with respect to the equilibrium C–J value, yet bounded by the CV lower limit. Between these two limits, the detonation wave undergoes a transition from transverse wave modes to shock-induced quasi-detonation modes and may be grossly described by the multiphase ZND model.

Hybrid Detonation

Although fine solid particles suspended in air are not sensitive to detonation due to a large transverse wave spacing, their combustion in gaseous detonation products may support so-called hybrid detonation and hybrid DDT. According to the analysis in the section on multiphase detonation theory, the necessary conditions for a weak detonation solution can be satisfied in inert or reactive particle–gas flow under an appropriate choice of physical and chemical properties of solid particles as well as reactive gas. A set of possible solutions can be realized by controlling the late particle reaction to meet rear flow or boundary conditions behind the gas reaction zone.

Experimentally, three most important hybrid detonation modes are shown here in aluminum particle–gas mixtures with a particle concentration ranging from 250 to 2000 g/m^3 observed in the 8-cm-diam tube [30–32]. In all three modes, a pressure wave or shock wave was formed in the gas detonation flow due to particle combustion, thus enhancing the impulse loading. Figure 22 displays a steady strong hybrid detonation in 500 g/m^3, 2 μm spherical aluminum particles suspended in $\phi = 0.8$ lean C_2H_2-air. The strong hybrid detonation is characterized by the leading shock front followed by a compression wave in the gas detonation zone, caused by sufficiently large heat release rate of the small particles within the gas reaction zone. This increases pressure and decreases detonation cell size with respect to the baseline gas detonation alone (Figs. 22 and 23) and therefore overdrives gas detonation. The detonation velocity is measured to be 1800 m/s, increased by 1.5% from the value of the baseline gas detonation. The secondary compression wave and its inclusion in the gas detonation zone can be more clearly resolved

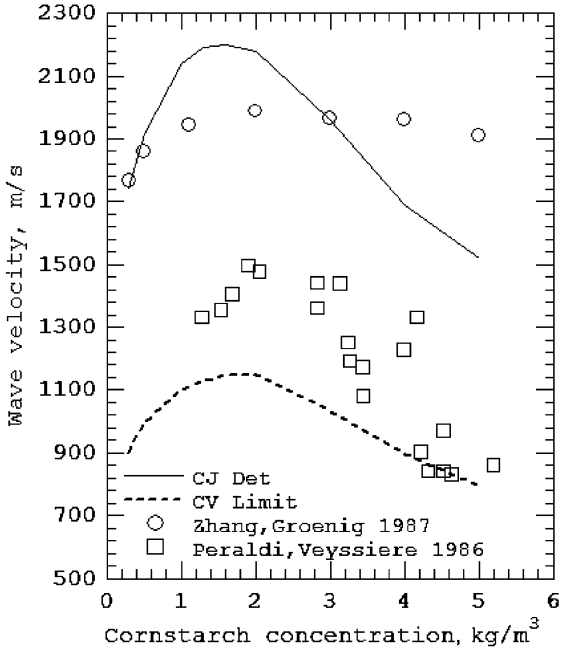

Fig. 21 Detonation and quasi-detonation velocities in cornstarch–oxygen mixtures in various diameter tubes.

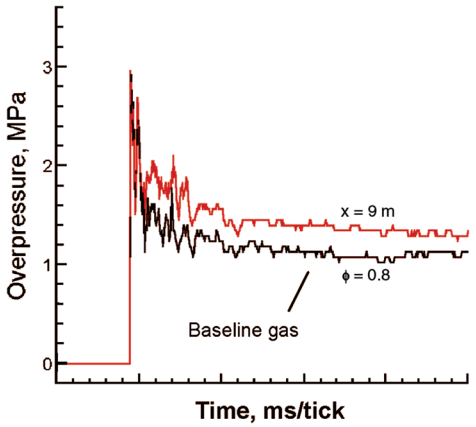

Fig. 22 Strong hybrid detonation in a mixture of $\phi = 0.8$ C_2H_2-air and 500 g/m^3, 2 μ aluminum particles.

through numerical simulations such as shown in Fig. 3a, where the compression wave penetrates two-thirds within the detonation zone of the baseline gas alone. Recent experimental results of Veyssiere and Ingignoli indicated that the mean detonation cell size can be reduced by 38% and the detonation velocity is increased by 4% when adding flaked aluminum particles to a lean hydrogen–air mixture [29].

When the aluminum particle size was increased to 10 μm, the particles behaved as inert within the gas reaction zone and particle heat release took place after the gas reaction zone. Therefore, a steady hybrid weak detonation wave resulted and its propagation along the 10 m tube length and comparison with the baseline gas detonation are shown in Figs. 24 and 25, respectively, from two experiments. This is the type-1 double-shock weak solution characterized by a two-shock

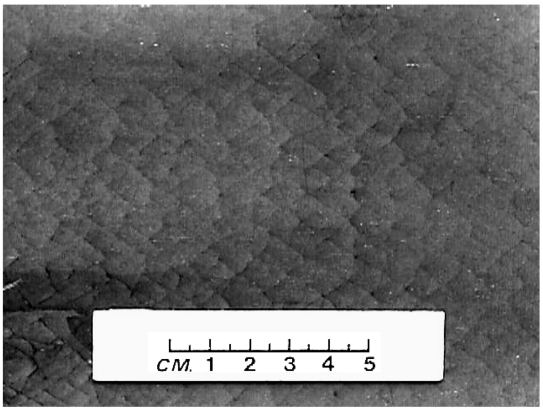

a) Cell size of λ = 7±2 mm for the hybrid mixture shown in Fig. 22

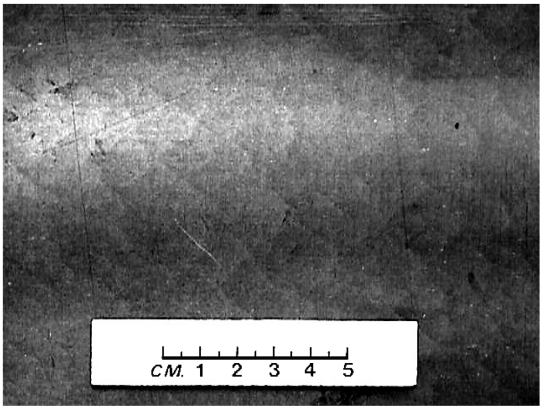

b) Cell size of λ = 8±2 mm for ϕ = 0.8 C_2H_2-air

Fig. 23 Cellular detonation structure for the strong hybrid detonation.

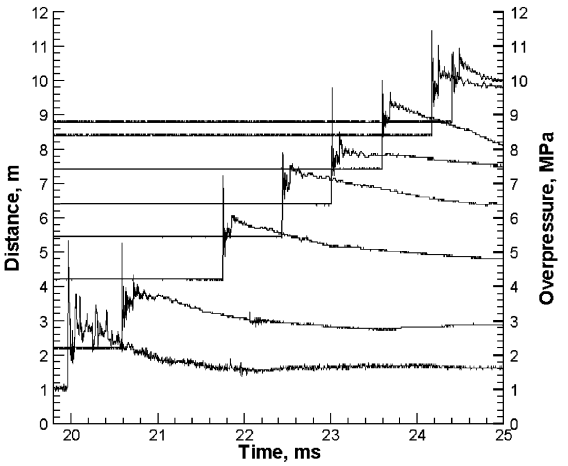

Fig. 24 Type-1 weak hybrid detonation in a mixture of $\phi = 0.8$ C_2H_2-air and 500 g/m^3, 10 μm atomized aluminum particles.

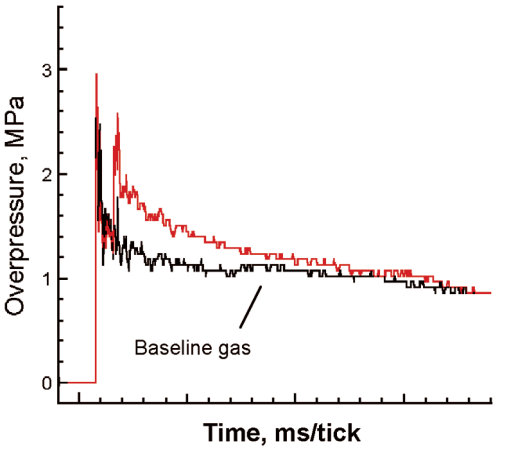

Fig. 25 Type-1 weak hybrid detonation for the hybrid mixture shown in Fig. 24.

structure, where the second shock behind the gaseous frozen sonic plane has the same velocity as the leading shock (Fig. 26). Aluminum combustion is in a deflagration mode for the large particle size. The apparent detonation cell size printed on the smoke foil is mainly governed by the gas detonation (Fig. 27), due to insignificant momentum and heat transferred to the large particles within the gas detonation zone. This cell size appears to provide little information about the sensitivity of aluminum ignition and combustion.

On further increasing the aluminum particle size to 22 μm to delay and reduce the heat release rate of the particles, a type-2 double-shock weak detonation was observed. This is characterized by two shock fronts, where the second front behind the gaseous frozen sonic plane has a velocity less than the leading front, as demonstrated in Figs. 28–30. Hence, the second shock recedes from the gas reaction zone to produce an ever-widening region of supersonic flow between the end of gas reaction zone and itself. Although rigorously speaking, the flow in this widening region in front of the second shock is unsteady, the experimental velocity of the second shock appears fairly steady as the wave propagates from $x = 4$ m to the end of the 10 m tube. Again, the detonation cell size recorded on the smoke foil apparently corresponds to that of the gas detonation, due to the large particles used.

The influence of the gaseous detonation parameters and products composition on the hybrid detonation was investigated through systematic experiments using 2–22 μm spherical aluminum particles in detonation of various equivalence ratios of acetylene–air, hydrogen–air, sensitized carbon monoxide–air, and ethylene–air

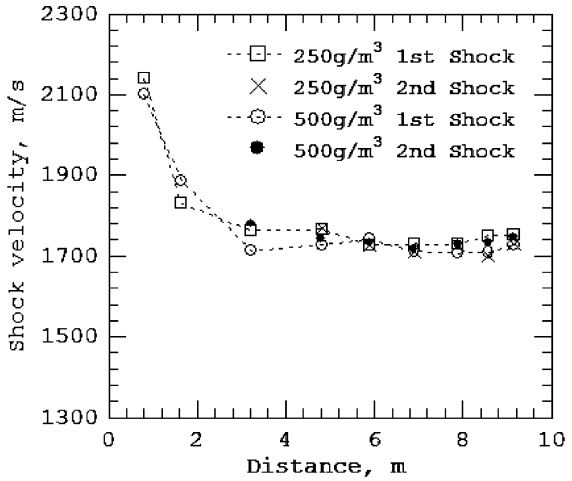

Fig. 26 First and second shock velocities vs propagation distance in mixtures of $\phi = 0.8$ C_2H_2-air and 10 μm atomized aluminum particles.

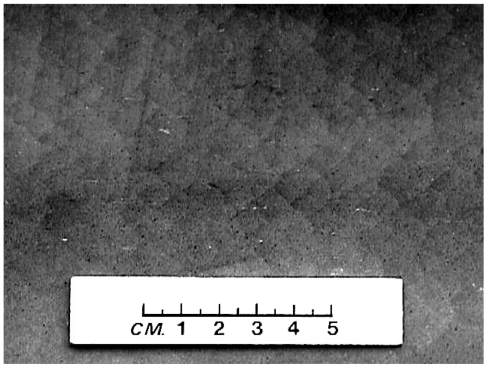

Fig. 27 Cellular detonation structure for the type-1 weak hybrid detonation for the hybrid mixture shown in Fig. 24.

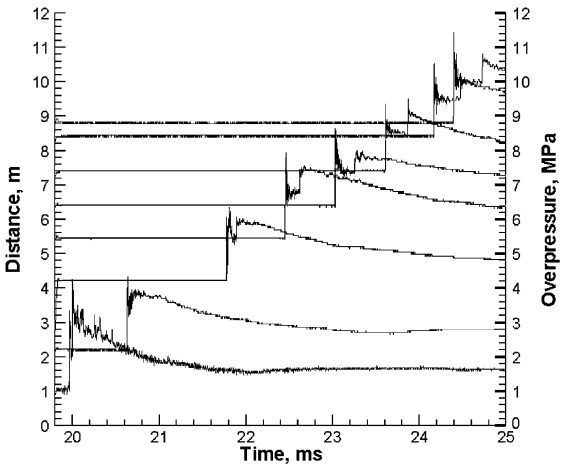

Fig. 28 Type-2 weak hybrid detonation in a mixture of $\phi = 0.8$ C_2H_2-air and 1000 g/m^3, 22 μm atomized aluminum particles.

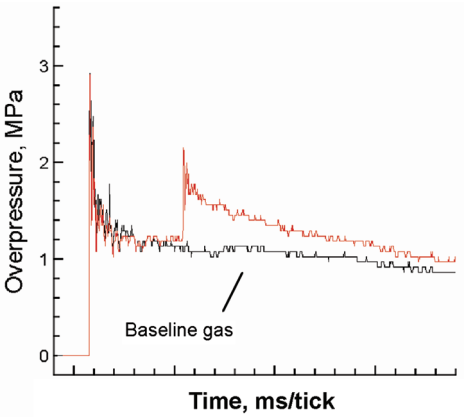

Fig. 29 Type-2 weak hybrid detonation in a mixture of $\phi = 0.8$ C_2H_2-air and 500 g/m^3, 22 μm atomized aluminum particles.

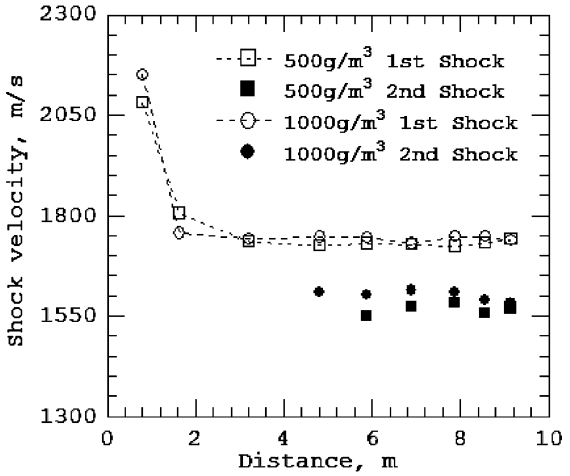

Fig. 30 Shock velocities vs propagation distance in mixtures of $\phi = 0.8$ C_2H_2-air and 22 μm atomized aluminum particles.

with detonation cell sizes ranging between 4 and 38 mm [30–32]. It was found that the double-shock detonation waves can propagate in detonation products with the presence of oxygen, water vapor, or carbon dioxide, but the second shock fails in detonation products dominated by carbon monoxide. These experiments further justified the theory stated in the section on multiphase detonation theory that the double-shock weak detonation waves strongly depend on the combination of the momentum and heat transferred to the particles within the gas reaction zone and the heat release rate of particles behind the gas reaction zone. By decreasing the heat release rate of particles through an increase in particle size or changing the products composition and parameters of gaseous detonation, the type-1 double-shock weak detonation was shifted to the type-2. A further decrease in the heat release rate of the particles resulted in further receding of the second shock with a weaker shock strength. An increase in initial pressure resulted in an increase in the heat release rate of the particles and therefore facilitated the steady hybrid detonation waves.

It is noticeable that the fuel–air gas detonation alone may not be sufficient to initiate combustion of relatively large particles quickly enough to form a secondary shock [31]. It was found that the secondary shock did not appear in the same particle–gas system with 22 μm aluminum particles shown in Figs. 28–30 until using 5 g condensed charge initiation, whereas the C_2H_2-air detonation was already initiated directly and propagating steadily under a 0.2 g charge mass. These results clearly indicate that the fuel–air detonation itself is insufficient to initiate and maintain a hybrid double-shock weak detonation wave involving large aluminum particles and that additional initiation charges are required. The double-wave hybrid detonation waves have also been observed recently in condensed-phase explosives with aluminum particles [130].

Deflagration-to-detonation transition in a dense solid particle–gas layer near a wall can generate a very significant pressure. Such a hybrid DDT was observed in the 8 cm tube filled with a 1 atm lean acetylene–air mixture and a 10 cm suspension of aluminum particles

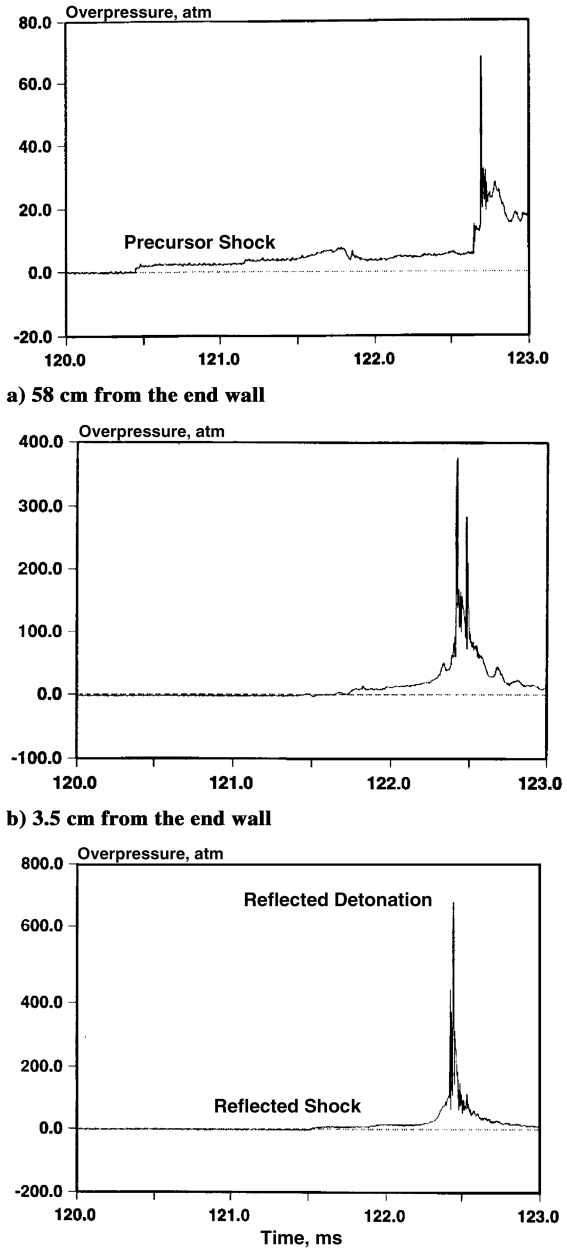

Fig. 31 DDT in 6.75% C_2H_2-air with a 10 cm dense aluminum particle suspension near the tube end wall.

with a concentration of 10 kg/m^3 located near the tube end wall [33]. DDT occurred after the wall reflection and the reflected detonation produced a wall peak pressure of 700 atm (Fig. 31). In comparison, a DDT after the wall reflection for the same gas system without particles achieved a wall peak pressure between 260 and 300 atm [33,131,132]. Thus, addition of a dense particle layer provides a pressure enhancement factor of more than two. The enhancement effect results from both the higher reflected gas pressures due to the multiple shock interactions with dense particles, and the mass and heat transferred from the subsequent particle combustion.

Conclusions

The recent efforts in pursuing clean experiments have led progress in the understanding of the fundamental mechanisms of detonation waves in dilute solid particle–gas flow. It appears that detonations in fine organic or metallic particles suspended in an oxidizing gas can be divided into heterogeneous detonation waves and quasi-detonation waves. The macroscopic propagation mechanisms for the heterogeneous detonation waves are similar to that for homogeneous gas mixtures, that is, the transverse waves in the single-head spinning or cellular structure provides the coupling between the shock and reaction. The difference is that the characteristic scale of detonation cell size for particle–gas mixtures is of at least one order of magnitude larger than that typically encountered in gas mixtures, due to the additional time scales introduced by the physical processes of mass, momentum, and heat transfer between the particles and the gas. The time scale of particle reaction is basic and leads to the main time scale for the mass transfer and therefore for the energy release of particles. On the other hand, the heterogeneous quasi-detonation waves that propagate in tubes much smaller than the characteristic detonation cell size are essentially shock-induced supersonic combustion waves without fully developed transverse wave structure. The quasi-detonation waves propagate at a shock velocity below the transverse wave mode detonations but above a lower limit characterized by the equilibrium constant volume combustion at the sonic plane. Although the quasi-detonation wave is unique for reactive particle–gas mixtures, presumably due to the distributed hot spots or local explosions induced by particles, more investigations are required to understand its propagation mechanisms.

Hybrid detonation waves occur in reactive particles suspended in a detonable gas. A variety of hybrid detonation modes can exist and the solution is a function of the gas reaction time scales and the additional time scales of the mass, momentum, and heat transfer between the particles and the gas. The rate of particle energy release, including its delay time and magnitude, represents a characteristic parameter to specify a possible solution. Among various modes, a strong hybrid detonation wave and two types of double-shock weak detonation waves are most important in practice, due to their enhancement to the gas detonation impulse loading. The strong hybrid detonation is characterized by the leading shock front followed by a compression wave resulting from particle combustion in the gas detonation zone, thus overdriving the gas detonation. The two types of double-shock weak detonation waves are featured by a two-shock structure where the second shock front, caused by the particle combustion behind the gas reaction zone, has a propagation velocity either the same as or less than the leading shock front, thus enhancing the impulse loading of the gas detonation. Whereas the strong hybrid detonation reduces the cell size of the baseline gas detonation, the cell sizes in the hybrid weak detonation waves are mainly governed by the gas detonation and provide little information about the sensitivity of aluminum ignition and combustion which often requires a strong initiation. The variety of hybrid detonation modes and their propagation mechanisms are still a subject of current research.

Although the fundamental studies of detonation in solid particle–gas flow have made significant progress, many problems remain to be resolved. The detonation velocity and pressure are experimentally available only for a few solid particle–gas mixtures. Few dynamic detonation parameters, including the ordinary cell size and critical initiation energy, have yet to be directly measured. Although the macroscopic mechanisms for the DDT, detonation onset, and propagation seem similar to the homogeneous gas detonation, the mechanisms of the heterogeneous detonation and quasi detonation in tubes cannot be fully established without mesoscale studies on the shock and gas flow interactions with the combustion dynamics of distributed particles, as well as the influence of the boundary layer. Though the heat release rate of particles under detonation conditions is a key parameter in controlling the detonation phenomena in solid particle–gas flow, there lack direct experimental measurements for a quantitative description of the reaction mechanism and heat release rate even for the popular aluminum particles under shock and detonation conditions. The reliability and predictability of two-phase continuum detonation theory and numerical modeling are currently mostly challenged by the uncertainty of ignition and reaction mechanisms of solid particles and, for dense solid particle–gas flow, the interphase interaction functions and the equations of state for solid particles. Experimental determination and mesoscale modeling would be two critical approaches in resolving these difficult issues.

Although the high-energy content of the solid particles and its combustibility in gaseous combustion products are attractive in the

propulsion applications, the large detonation length scale of reactive particle-oxidizing gas systems may not be a favorite for stable operation of a size-limited or time-limited propulsion engine and apparatus. However, the high-energy release and relatively fast reaction of small particles are promising in a variety of other combustion modes, such as hybrid detonation waves, quasi-detonation waves, high-speed deflagrations, and constant volume explosions, apart from the constant pressure combustion of the classic rocket propulsion.

Acknowledgments

The author is greatly indebted to Hans Grönig. The author wishes to give special thanks to John Lee, Martin Sichel, Peter Wolanski, Herbert Oliver, A. van de Ven, Gihui Geng, Stephen Murray, Paul Thibault, Julian Lee, Peter Greilich, Akio Yoshinaka, Keith Gerrard, Arnie Nickel, and Darrel Boechler. The author would also like to acknowledge the useful comments made by the referees.

References

[1] Strauss, W. A., "Investigation of the Detonation of Aluminum Powder-Oxygen Mixtures," *AIAA Journal*, Vol. 6, 1968, pp. 1753–1757.

[2] Cybulski, W. B., "Detonation of Coal Dust," *Bulletin of the Polish Academy of Science*, Vol. 19, 1971, pp. 37–41.

[3] Nettleton, M. A., and Stirling, R., "Detonations in Suspensions of Coal Dust in Oxygen," *Combustion and Flame*, Vol. 21, 1973, pp. 307–314.

[4] Bartknecht, W., *Explosionen*, Springer–Verlag, Berlin, 1978, pp. 5–72.

[5] Kauffman, C. W., Wolanski, P., Ural, E., Nicholls, J. A., and Van Dyke, R., "Shock Initiated Combustion of Grain Dust," *Proceedings of International Symposium on Grain Dust*, Manhattan, Kansas, 1979, pp. 164–190.

[6] Kauffman, C. W., Wolanski, P., Arisoy, A., Adams, P. R., Maker, B. N., and Nicholls, J. A., "Dust, Hybrid, and Dusty Detonations," *Dynamics of Shock Waves, Explosions, and Detonations*, edited by Bowen, J. R., Manson, N., Oppenheim, A. K., and Soloukhin, R. I., Vol. 94, Progress in Astronautics and Aeronautics, AIAA, New York, 1984, pp. 221–240.

[7] Fangrat, J., Glinka, W., Wolanski, P., and Wolinski, M., "Detonation Structure in Organic Dust-Oxygen Mixtures," *Archivum combustionis / Polska Akademia Nauk, Komitet Termodynamiki i Spalania*, Vol. 7, 1987, pp. 321–332.

[8] Wolanski, P., "Deflagration and Detonation of Dust Mixtures," *Dynamics of Deflagration and Reaction Systems: Heterogeneous Combustion*, edited by Kuhl, A. L., Leyer, J. C., Borisov, A. A., and Sirignano, W. A., Vol. 132, Progress in Astronautics and Aeronautics, AIAA, New York, 1991, pp. 3–31.

[9] Veyssiere, B., "Structure of the Detonations in Gaseous Mixtures Containing Aluminium Particles in Suspension," *Dynamics of Explosions*, edited by Bowen, J. R., Leyer, J. C., and Soloukhin, R. I., Vol. 106, Progress in Astronautics and Aeronautics, AIAA, New York, 1986, pp. 522–544.

[10] Peraldi, O., and Veyssiere, B., "Experimental Study of Detonations in Starch Particle Suspensions with O_2/N_2, H_2/O_2, and C_2H_4/O_2 Mixtures," in *Dynamics of Explosions*, edited by Bowen, J. R., Leyer, J. C., and Soloukhin, R. I., Vol. 106, Progress in Astronautics and Aeronautics, AIAA, New York, 1986, pp. 490–504.

[11] Tulis, A. J., and Selman, J. R., "Detonation Tube Studies of Aluminum Particles Dispersed in Air," *Proceedings of the 19th International Symposium on Combustion*, Combustion Inst., Pittsburgh, PA, 1982, pp. 655–663.

[12] Gardner, B. R., Winter, R. J., and Moore, M. J., "Explosion Development and Deflagration-to-Detonation Transition in Coal Dust/Air Suspensions," *Proceedings of the 21st International Symposium on Combustion*, Combustion Inst., Pittsburgh, PA, 1986, pp. 335–343.

[13] Zhang, F., and Grönig, H., "Spin Detonation in Reactive Particles-Oxidizing Gas Flow," *Physics of Fluids A*, Vol. 3, 1991, pp. 1983–1990.

[14] Zhang, F., and Grönig, H., "Two-Headed Detonation in Reactive Particle-Oxidizing Gas Flow," *Physics of Fluids A*, Vol. 4, 1992, pp. 2308–2315.

[15] Zhang, F., Greilich, P., and Grönig, H., "Propagation Mechanism of Dust Detonations," *Shock Waves*, Vol. 2, 1992, pp. 81–88.

[16] Grönig, H., "Dust Detonations," *JSME International Journal, Series B (Fluids and Thermal Engineering)*, Vol. 40, 1997, pp. 1–15.

[17] Borisov, A. A., Khasainov, B. A., Saneev, E. L., Formin, I. B., Khomik, S. V., and Veyssiere, B., "On the Detonation of Aluminum Suspensions in Air and in Oxygen," *Dynamic Structure of Detonation in Gaseous and Dispersed Media*, edited by Borisov, A. A., Kluwer, Dordrecht, The Netherlands, 1991, pp. 215–253.

[18] Pu, Y. K., Li, K. Y., and Jarosinski, J., "Transition to Detonation in Aluminum Dust-Air Mixtures under Weak Ignition Conditions," *Proceedings of the 16th International Colloquium on the Dynamics of Explosions and Reactive Systems*, AGH, Cracow, Poland, 1997, pp. 259–262.

[19] Zhang, F., Grönig, H., and van de Ven, A., "DDT and Detonation Waves in Dust-Air Mixtures," *Shock Waves*, Vol. 11, 2001, pp. 53–71.

[20] Zhang, F., Murray, S. B., Gerrard, K. B., "Aluminium Dust-Air Detonation at Elevated Pressures," *Shock Waves*, edited by Jiang, Z., Tsinghua Univ. Press and Springer–Verlag, Heidelberg, Germany, 2004, pp. 795–800.

[21] Lee, J. H. S., "Dust Explosion: an Overview," *Shock Tubes and Waves*, edited by Grönig, H., Wiley–VCH, Weinheim, Germany, 1988, pp. 31–38.

[22] Li, Y.-C., Alexander, C. G., Wolanski, P., Kauffman, C. W., and Sichel, M., "Experimental Investigations of Accelerating Flames and Transition to Detonation in Layered Grain Dust," *Dynamic Aspects of Explosion Phenomena*, edited by Kuhl, A. L., Leyer, J.-C., and Borisov, A. A., Vol. 154, Progress in Astronautics and Aeronautics, AIAA, New York, 1993, pp. 170–184.

[23] Veyssiere, B., and Manson, N., "Sur L'Existence d'un Second Front de Détonation des Mélanges Biphasiques Hydrogène-Oxygène-Azote-Particules d'Aluminium," *Note aux Comptes Rendus de l'Académie des Sciences*, Vol. 295, No. 2, 1982, pp. 335–338.

[24] Veyssiere, B., "Double-Front Detonations in Gas-Solid Particles Mixtures," *Dynamics of Shock Waves, Explosions, and Detonations*, edited by Bowen, J. R., Manson, N., Oppenheim, A. K., and Soloukhin, R. I., Vol. 94, Progress in Astronautics and Aeronautics, AIAA, New York, 1984, pp. 264–276.

[25] Afanasieva, L. A., Levin, V. A., and Tunik, Y. V., "Multifront Combustion of Two-Phase Media," *Dynamics of Shock Waves, Explosions, and Detonations*, edited by Bowen, J. R., Manson, N., Oppenheim, A. K., and Soloukhin, R. I., Vol. 87, Progress in Astronautics and Aeronautics, AIAA, New York, 1983, pp. 394–413.

[26] Khasainov, B. A., and Veyssiere, B., "Steady, Plane, Double-Front Detonations in Gaseous Detonable Mixtures Containing a Suspension of Aluminium Particles," edited by Kuhl, A. L., Vol. 114, Progress in Astronautics and Aeronautics, AIAA, New York, 1988, pp. 284–299.

[27] Veyssiere, B., and Khasainov, B. A., "Structure and Multiplicity of Detonation Regimes in Heterogeneous Hybrid Mixtures," *Shock Waves*, Vol. 4, 1995, pp. 171–186.

[28] Wolinski, M., Teodorczyk, A., Wolanski, P., Klemens, R., Sichel, M., and Nettleton, M., "Hybrid Detonations in Oats Dust Clouds in methane–air Mixtures," *Combustion Science and Technology*, Vol. 120, 1996, pp. 39–53.

[29] Veyssiere, B., and Ingignoli, W., "Existence of the Detonation Cellular Structure in Two-Phase Hybrid Mixtures," *Shock Waves*, Vol. 12, 2003, pp. 291–299.

[30] Zhang, F., Murray, S. B., and Gerrard, K. B., "Hybrid Detonations in Aluminum Dust-Gas Mixtures," *Proceedings of the 19th International Colloquium on the Dynamics of Explosions and Reactive Systems*, Aoyama Gakuin Univ., Kanagawa, Japan, 2003, 4-9901744-1-0, pp. 167.1–167.4.

[31] Zhang, F., Murray, S. B., and Gerrard, K. B., "Hybrid Detonation Waves in Heterogeneous Explosive Mixtures," *Proceedings of the 18th International Symposium on Military Aspects of Blast and Shock*, Bad Reichenhall, Germany, 2004, Paper for Special Interest, pp. 1–14.

[32] Zhang, F., Murray, S. B., and Gerrard, K. B., "Hybrid Detonation Waves," *Proceedings of the 20th International Colloquium on the Dynamics of Explosions and Reactive Systems*, McGill Univ., Montreal, 2005, pp. 217.1–217.12.

[33] Zhang, F., Thibault, P. A., and Murray, S. B., "Transition from Deflagration to Detonation in an End Multiphase Slug," *Combustion and Flame*, Vol. 114, 1998, pp. 13–25.

[34] Davis, W. C., Craig, B. G., and Ramsay, J. B., "Failure of the Chapman–Jouguet Theory for Liquid and Solid Explosives," *Physics of Fluids*, Vol. 8, 1965, pp. 2169–2182.

[35] Vasiliev, A. A., Gavrilenko, T. P., and Topchian, M. E., "On the Chapman–Jouguet Surface in Multi-Headed Detonations," *Acta Astronautica*, Vol. 17, 1972, pp. 499–502.

[36] Edwards, D. H., Jones, A. T., and Phillips, D. E., "The Location of the Chapman–Jouguet Surface in a Multiheaded Detonation Wave,"

Journal of Physics D: Applied Physics, Vol. 9, 1976, pp. 1331–1342.
[37] Weber, M., and Olivier, H., "The Thickness of Detonation Waves Visualized by Slight Obstacles," *Shock Waves*, Vol. 13, 2003, pp. 351–365.
[38] Fried, L. E., Howard, W. M., and Souers, P. C., "CHEETAH 2.0 User's Manual," Lawrence Livermore National Lab. Rept. UCRL-MA-117541, 1998.
[39] Zhang, F., Thibault, P. A., and Link, R., "Shock Interaction with Solid Particles in Condensed Matter and Related Momentum Transfer," *Proceedings of the Royal Society of London A*, Vol. 459, 2003, pp. 705–726.
[40] Zeldovich, Ya. B., and Kompaneets, A. S., *Theory of Detonation*, Academic Press, London, 1960, pp. 133–205; translated from the original Russian edition published in Moscow, 1955.
[41] Wood, W. W., and Kirkwood, J. G., "Diameter Effect in Condensed Explosives: The Relation Between Velocity and Radius of Curvature of the Detonation Wave," *Journal of Chemical Physics*, Vol. 22, 1954, pp. 1920–1924.
[42] Kuznetsov, N. M., "Nonuniqueness and Stability of Detonation Modes," *Soviet Physics, JETP*, Vol. 25, 1967, pp. 199–204.
[43] Erpenbeck, J. J., "Stability of Idealized One-Reaction Detonations," *Physics of Fluids (1958-1988)*, Vol. 7, 1964, pp. 684–696.
[44] Fickett, W., and Wood, W. W., "Flow Calculations for Pulsating One-Dimensional Detonations," *Physics of Fluids*, Vol. 9, 1966, pp. 903–916.
[45] Abouseif, G. E., and Toong, T. Y., "Theory of Unstable One-Dimensional Detonations," *Combustion and Flame*, Vol. 45, 1982, pp. 67–94.
[46] Lee, H. I., and Stewart, D. S., "Calculation of Linear Detonation Instability: One-Dimensional Instability of Planer Detonations," *Journal of Fluid Mechanics*, Vol. 216, 1990, pp. 103–132.
[47] Sharpe, G. J., "Linear Stability of Pathological Detonations," *Journal of Fluid Mechanics*, Vol. 401, 1999, pp. 311–338.
[48] Bourlioux, A., Majda, A. J., and Roytburd, V., "Theoretical and Numerical Structure of Unstable One-Dimensional Detonations," *SIAM Journal on Applied Mathematics*, Vol. 51, 1991, pp. 303–343.
[49] He, L., and Lee, J. H. S., "The Dynamics Limit of One-Dimensional Detonations," *Physics of Fluids*, Vol. 7, 1995, 1151–1158.
[50] Ng, H. D., and Lee, J. H. S., "Direct Instability of Detonation with a Multi-Step Reaction Scheme," *Journal of Fluid Mechanics*, Vol. 476, 2003, pp. 179–211.
[51] Wolanski, P., Lee, D., Sichel, M., Kauffman, C. W., and Nicholls, J. A., "The Structure of Dust Detonations," *Dynamics of Shock Waves, Explosions, and Detonations*, edited by Bowen, J. R., Manson, N., Oppenheim, A. K., and Soloukhin, R. I., Vol. 94, Progress in Astronautics and Aeronautics, AIAA, New York, 1984, pp. 241–263.
[52] Lee, D., and Sichel, M., "The Chapman–Jouguet Condition and Structure of Detonation in Dust-Oxidizer Mixtures," *Dynamics of Explosions*, edited by Bowen, J. R., Leyer, J. C., and Soloukhin R. I., Vol. 106, Progress in Astronautics and Aeronautics, AIAA, New York, 1986, pp. 505–521.
[53] Baer, M. R., and Nunziato, J. W., "A Two-Phase Mixture Theory for the Deflagration-to-Detonation Transition (DDT) in Reactive Granular Materials," *International Journal of Multiphase Flow*, Vol. 12, 1986, pp. 861–889.
[54] Powers, J. M., Stewart, D. S., and Krier, H., "Theory of Two-Phase Detonations Part 1: Modeling," *Combustion and Flame*, Vol. 80, 1990, pp. 264–279.
[55] Powers, J. M., Stewart, D. S., and Krier, H., "Theory of Two-Phase Detonations Part 2: Structure," *Combustion and Flame*, Vol. 80, 1990, pp. 280–303.
[56] Fan, B. C., and Sichel, M., "A Comprehensive Model for the Structure of Dust Detonations," *Proceedings of the 22nd International Symposium on Combustion*, Combustion Inst., Pittsburgh, PA, 1988, pp. 1741–1750.
[57] Gelfand, B. E., Frolov, S. M., and Nettleton, M. A., "Gaseous Detonations: A Selective Review," *Progress in Energy and Combustion Science*, Vol. 17, 1991, pp. 327–371.
[58] Nigmatulin, R. I., *Dynamics of Multiphase Media*, Hemisphere, NY, Vol. 1, 1991, pp. 358–372.
[59] Zhang, F., "Numerical Studies of Detonation Propagation in Mixtures of Combustible Gasses and Inert Dust," *The 2nd Conference of the CFD Society of Canada*, edited by Gottlieb, J. J., and Ethier, C. R., Univ. of Toronto, Toronto, 1994, pp. 261–268.
[60] Zhang, F., Frost, D. L., Thibault, P. A., and Murray, S. B., "Explosion Dispersal of Solid Particles," *Shock Waves*, Vol. 10, 2001, pp. 431–443.
[61] Kapila, A. K., Son, S. F., Bdzil, J. B., Menikoff, R., and Stewart, D. S., "Two-Phase Modeling of DDT, Structure of the Velocity-Relaxation Zone," *Physics of Fluids*, Vol. 9, 1997, pp. 3885–3897.
[62] Korobeinikov, V., "Formation of Zone with High Particle Concentrations in Dusty Gasses," *Dynamics of Deflagration and Reactive Systems*, edited by Kuhl, A. L., Leyer, J.-C., Borisov, A. A., and Sirignano, W. A., Vol. 132, Progress in Astronautics and Aeronautics, AIAA, New York, 1991, pp. 287–292.
[63] Zhang, F., and Lee, J. H. S., "Friction-Induced Oscillatory Behavior of One-Dimensional Detonations," *Proceedings of the Royal Society of London A*, Vol. 446, 1994, pp. 87–105.
[64] Zhang, F., Chue, R. S., Frost, D. L., Lee, J. H. S., Thibault, P., and Yee, C., "Effects of Area Change and Friction on Detonation Stability in Supersonic Ducts," *Proceedings of the Royal Society of London A*, Vol. 449, 1995, pp. 31–49.
[65] Fickett, W., and Davis, W. C., *Detonation*, Univ. of California Press, Berkeley, CA, 1979, pp. 153–191.
[66] Hayashi, A. K., Fuyuto, T., and Fujiwara, T., "Triple-Shock Structure in Dusty Gas Detonations," *Proceedings of the 20th International Symposium on Shock Waves*, edited by Sturtevant, B., Shepherd, J. E., and Hornung, H. G., Vol. 2, World Scientific, London, 1996, pp. 1071–1076.
[67] Uphoff, U., Hanel, D., and Roth, P., "Influence of Reactive Particles on the Formation of a One-Dimensional Detonation Wave," *Combustion Science and Technology*, Vol. 110–111, 1995, pp. 419–441.
[68] Khasainov, B. A., Veyssiere, B., and Ingignoli, W., "Numerical Simulation of Detonation Cell Structure in Hydrogen-Air Mixture Loaded by Aluminum Particles," *High-Speed Deflagration and Detonation: Fundamentals and Control*, edited by Roy, G., Frolov, S., Netzer, D., and Borisov, A., ELEX-KM, Moscow, 2001, pp. 163–174.
[69] Fedorov, A. V., and Khmel, T. A., "Types and Stability of Detonation Flows of Aluminum Particles in Oxygen," *Fizika Goreniya Vzryva*, Vol. 32, 1996, pp. 74–85.
[70] Fedorov, A. V., and Khmel, T. A., "Interaction of Detonation and Rarefaction Waves in Aluminum Particles Dispersed in Oxygen," *Fizika Goreniya Vzryva*, , Vol. 33, 1997, pp. 102–110.
[71] Fedorov, A. V., and Khmel, T. A., "Mathematical Modeling of Detonation of Aluminum Powder in Oxygen with Allowance for Velocity Nonequilibrium of the Particles," *Fizika Goreniya Vzryva*, Vol. 33, 1997, pp. 80–91.
[72] Fedorov, A. V., and Khmel, T. A., "Determination of Nonideal Self-Sustained Detonation Regimes of Aluminum Particles in Air," *Fizika Goreniya Vzryva*, Vol. 34, 1998, pp. 95–102.
[73] Benkiewicz, K., and Hayashi, A. K., "One-Dimensional Parametric Studies of an Aluminum-Dust Combustion Model for Numerical Simulations of Detonation Waves," *AIAA Journal*, Vol. 44, No. 3, 2006, pp. 608–619.
[74] Ripley, R., Zhang, F., Lien, F. S., "Shock Interaction of Metal Particles in Condensed Explosive Detonation," *14th APS International Conference on Shock Compression of Condensed Matter*, *Shock Compression of Condensed Matter—2005*, edited by Furnish, M. D., Gupta, Y. M., and Forbes, J. W., American Inst. of Physics, Melville, NY (to be published).
[75] Rudinger, G., *Fundamentals of Gas-Particle Flow*, Elsevier, Amsterdam, 1980, pp. 76–85.
[76] Zhang, F., and Grönig, H., "Detonability of Organic Dust-Air Mixtures," *Dynamic Aspects of Explosion Phenomena*, edited by Kuhl, A. L., Leyer, J. C., Borisov, A. A., and Sirignano, W. A., Vol. 154, Progress in Astronautics and Aeronautics, AIAA, New York, 1993, pp. 195–215.
[77] Zhang, F., and Grönig, H., "Transition to Detonation in Cornstarch Dust-Oxygen and Air Mixtures," *Combustion and Flame*, Vol. 86, 1991, pp. 21–32.
[78] Urtiew, P. A., and Oppenheim, A. K., "Experimental Observation of the Transition to Detonation on an Explosive Gas," *Proceedings of the Royal Society of London A*, Vol. 295, 1966, pp. 13–29.
[79] Lee, J. H. S., and Moen, I. O., "The Mechanism of Transition from Deflagration to Detonation in Vapor Explosions," *Progress in Energy and Combustion Science*, Vol. 6, 1980, p. 359.
[80] Dove, J. E., and Wagner, H. Gg., "A Photographic Investigation of the Mechanisms of Spinning Detonation," *Proceedings of the 8th International Symposium on Combustion*, Combustion Inst., Pittsburgh, PA, 1960, pp. 589–600.
[81] Manson, N., "Propagations des Detonations et des Deflagrations dans les Melanges Gaseaux," L'Office National d'Etudes et des Recherches Aeronautics Et Inst. France Des Pétroles, Paris, *Comptes Rendus Hebdomadaires des Seances de l'Academie des Sciences* Vol. 222, 1947, pp. 46–51.
[82] Denisov, Y. N., and Troshin, Y. K., "Structure of Gaseous Detonation in Tubes," *Zhurnal Tekhnicheskoi Fiziki (Soviet Physics–Technical*

Physics), Vol. 30, 1960, pp. 450–459.
[83] Duff, R. E., "Investigation of Spinning Detonation and Detonation Stability," *Physics of Fluids*, Vol. 4, 1961, pp. 1427–1433.
[84] Voitsekhovskii, B. V., Mitrofanov, V. V., and Topchian, M. E., "Structure of a Detonation Front in Gases," *Izdatel'stvo Sibirskogo Otdeleniya Art SSSR*, 1963.
[85] Schott, G. L., "Observations of the Structure of Spinning Detonation," *Physics of Fluids*, Vol. 8, 1965, pp. 850–865.
[86] Mitrofanov, V. V., and Soloukhin, R. I., "The Diffraction of Multi-Front Detonation Waves," *Soviet Physics, Doklady*, Vol. 9, 1965, pp. 1055–1058.
[87] Strehlow, R. A., "The Nature of Transverse Waves in Detonations," *Acta Astronautica*, Vol. 14, 1969, pp. 539–548.
[88] Lundstrom, E. A., and Oppenheim, A. K., "On the Influence of Nonsteadiness on the Thickness of the Detonation Wave," *Proceedings of the Royal Society of London A*, Vol. 310, 1969, p. 463.
[89] Edwards, D. H., Hooper, G., Job, E. M., and Parry, D. J., "The Behavior of the Frontal and Transverse Shock in Gaseous Detonation Waves," *Acta Astronautica*, Vol. 15, 1970, p. 323.
[90] Strehlow, R. A., and Crooker, A. J., "The Structure of Marginal Detonation Waves," *Acta Astronautica*, Vol. 1, 1974, pp. 303–315.
[91] Lee, J. H. S., "Dynamic Parameters of Gaseous Detonations," *Annual Review of Fluid Mechanics*, Vol. 16, 1984, pp. 311–336.
[92] Shepherd, J. E., Pintgen, F., Austin, J. M., and Eckett, C. A., "The Structure of the Detonation Front in Gases," AIAA Paper 2002-0773, 2002.
[93] Shepherd, J. E., "Detonation: A Look Behind the Front," *Proceedings of the 19th International Colloquium on the Dynamics of Explosions and Reactive Systems*.
[94] van de Ven, A., "Staubdetonationen in einer Tohrleitung mit 300 mm Durchmesser," Dissertation, RWTH Aachen Shock Wave Lab., Verlag, Aachen, Germany, 1998.
[95] Zeldovich, Ya. B., Kogarko, S. M., and Simonov, M. N., "An Experimental Investigation of Spherical Detonation of Gases," *Soviet Physics–Technical Physics*, Vol. 1, 1956, pp. 1689–1713.
[96] Moen, I. O., Sulmistras, A., Thomas, G. O., Bjerketvedt, D., and Thibault, P. A., "Influence of Cellular Regularity on the Behavior of Gaseous Detonations," *Dynamics of Explosions*, edited by Bowen, J. R., Leyer, J. C., and Soloukhin, R. I., Vol. 106, Progress in Astronautics and Aeronautics, AIAA, New York, 1986, pp. 220–243.
[97] Moen, I. O., Donato, M., Knystautas, R., and Lee, J. H., "The Influence of Confinement on the Propagation of Detonations near the Detonability Limits," *Proceedings of the 18th International Symposium on Combustion*, Combustion Inst., Pittsburgh, PA, 1981, pp. 1615–1622.
[98] Benedick, W. B., Guirao, C. M., Knystautas, R., and Lee, J. H., "Critical Charge for Direct Initiation of Detonation in Gaseous Fuel-Air Mixtures," *Dynamics of Explosions*, edited by Bowen, J. R., Leyer, J. C., and Soloukhin, R. I., Vol. 106, Progress in Astronautics and Aeronautics, AIAA, New York, 1986, pp. 181–202.
[99] Lee, J. H. S., Knystautas, R., and Guirao, C., "The Link Between Cell Size, Critical Tube Diameter, Initiation Energy, and Detonability Limits," *Fuel-Air Explosions*, edited by Lee, J. H. S., and Guirao, C. M., Univ. of Waterloo Press, Waterloo, Canada, 1982, pp. 157–187.
[100] Vasil'ev, A. A., "Gaseous Fuels and Detonation Hazards," edited by Eisenreich, N. *Proceedings of 28th ICT Conference*, Karlsruhe, Germany, 1997, pp. 50.1–50.14.
[101] Kogarko, S. M., and Zeldovich, Ya. B., "On Detonation of Gas Mixtures," *Doklady Akademii Nauk SSSR (Soviet Physics–Doklady*, Vol. 63, 1948, pp. 553–556.
[102] Shchelkin, K. I., and Troshin, Ya. K., *Gasdynamics of Combustion*, Academy of Sciences, Moscow; translated by Kuvshinoff, B. W. and Holtschlag, L., Mono Book Corp., Baltimore, MD, 1965.
[103] Strehlow, R. A., and Engel, C. D., "Transverse Waves in Detonation 2: Structure and Spacing in H_2-O_2, C_2H_2-O_2, c_2h_4-o_2, and CH_4-O_2 Systems," *AIAA Journal*, Vol. 7, 1969, pp. 492–496.
[104] Friedman, R., and Macek, A., "Ignition and Combustion of Aluminum Particles in Hot Ambient Gases," *Combustion and Flame*, Vol. 6, 1962, pp. 9–19.
[105] Macek, A., "Fundamentals of Combustion of Single Aluminum and Beryllium Particles," *Proceedings of the 11th International Symposium on Combustion*, Combustion Inst., Pittsburgh, PA, 1967, pp. 203–217.
[106] Fontijn, A., and Felder, W., "HTFFR Kinetic Studies of $Al + CO_2 \rightarrow AlO + CO$ from 300 to 1800 K, a Non-Arrenhius Reaction," *Journal of Chemical Physics*, Vol. 67, 1977, p. 1561.
[107] King, M. K., "Modeling of Single Particle Aluminum Combustion in CO_2-N_2 Atmospheres," *Proceedings of the 17th International Symposium on Combustion*, Combustion Inst., Pittsburgh, PA, 1978, pp. 1317–1328.
[108] Gurevich, M. A., Lapkina, K. I., and Ozerov, E. S., "Ignition Limit of Aluminum Particles," *Combustion, Explosion and Shock Waves*, Vol. 6, No. 2, 1970, pp. 172–175.
[109] Davis, A., "Solid Propellants: The Combustion of Particles of Metal Ingredients," *Combustion and Flame*, Vol. 7, 1963, pp. 227–234.
[110] Pokhil, P. F., Belyayev, A. F., Frolov, Y. V., Logachev, V. S., and Kotkov, A. I., *Combustion of Powdered Metal in Active Media*, Nauka, Russia, 1972; also U.S. Air Force Foreign Technology Div. Translation FTD-MT-24-551-73.
[111] Foelsche, R. O., Burton, R. I., and Krier, H., "Ignition and Combustion of Aluminum Particles in $H_2/O_2/N_2$ Combustion Products," *Journal of Propulsion and Power*, Vol. 117, 1998, pp. 1001–1008.
[112] Melcher, J. C., Burton, R. L., Krier, H., "Combustion of Aluminum Particles in Solid Rocket Motor Flows," *Solid Propellant Chemistry, Combustion, and Motor Interior Ballistics*, edited by Yang, V., Brill, T. B., and Ren, W. Z., Vol. 185, Progress in Astronautics and Aeronautics, AIAA, Reston, VA, 2000, pp. 723–747.
[113] Melcher, J. C., Krier, H., and Burton, R. L., "Burning Aluminum Particles Inside a Laboratory-Scale Solid Rocket Motor," *Journal of Propulsion and Power*, Vol. 18, 2002, pp. 631–640.
[114] Glassman, I., *Combustion*, Academic Press, New York, 1977, pp. 168–193.
[115] Lee, J. J., and Zhang, F., "Burning Properties of Aluminum in H_2O or CO_2 Gas," *Proceedings of the 20th International Colloquium on the Dynamics of Explosions and Reactive Systems*, McGill Univ., Montreal, 2005, pp. 179.1–179.7.
[116] Borisov, A. A., Gelfand, B. E., Timofeev, E. I., Tsyganov, S. A., and Khomic, S. V., "Ignition of Dust Suspensions Behind Shock Waves," *Dynamics of Shock Waves, Explosions, and Detonations*, edited by Bowen, J. R., Manson, N., Oppenheim, A. K., and Soloukhin R. I., Vol. 96, Progress in Astronautics and Aeronautics, AIAA, New York, 1984, pp. 332–339.
[117] Tanguay, V., Goroshin, S., Higgins, A., Yoshinaka, A., and Zhang, F., "Reaction of Metal Particles in Gas-Phase Detonation Products," *Proceedings of the 20th International Colloquium on the Dynamics of Explosions and Reactive Systems*, McGill Univ., Montreal, 2005, pp. 225.1–225.16.
[118] Fox, T. W., Rackett, C. W., and Nicholls, J. A., "Shock Wave Ignition of Magnesium Powders," *Proceedings of the 11th International Symposium on Shock Waves and Tubes*, 1978, pp. 262–268.
[119] Boiko, V. M., Fedorov, A. V., Formin, V. M., Papyrin, A. N., and Soloukhin, R. I., "Ignition of Small Particles Behind Shock Waves," *Dynamics of Shock Waves, Explosions, and Detonations*, edited by Bowen, J. R., Manson, N., Oppenheim, A. K., and Soloukhin, R. I., Vol. 87, Progress in Astronautics and Aeronautics, AIAA, New York, 1982, pp. 71–87.
[120] Sichel, M., Baek, S. W., Kauffman, C. W., Maker, B., Nicholls, J. A., and Wolanski, P., "The Shock Wave Ignition of Dusts," *AIAA Journal*, Vol. 23, 1985, pp. 1374–1380.
[121] Geng, J. H., van de Ven, A., Zhang, F., and Grönig, H., "Shock-Induced Ignition Delay of Cornstarch Dust," *Proceedings of the 5th International Colloquium on Dust Explosion*, edited by Wolanski, P., Warsaw Univ., Warsaw, 1993, pp. 321–328.
[122] Servaites, J., Krier, H., Melcher, J. C., and Burton, R. L., "Ignition and Combustion of Aluminum Particles in Shocked $H_2O/O_2/Ar$ and $CO_2/O_2/Ar$ Mixtures," *Combustion and Flame*, Vol. 125, 2001, pp. 1040–1054.
[123] Fay, J. A., "Two-Dimensional Detonations: Velocity Deficits," *Physics of Fluids*, Vol. 2, 1959, pp. 283–289.
[124] Manson, N., Brochet, C., Brossard, J., and Pujol, Y., "Vibratory Phenomena and Instabilities of Self-Sustained Detonations in Gases," *Proceedings of the 9th International Symposium on Combustion*, Academic Press, New York, 1963, pp. 461–469.
[125] Dabora, E. K., Nicholls, J. A., and Morrison, R. B., "The Influence of a Compressible Boundary on the Propagation of Gaseous Detonations," *Proceedings of the 10th International Symposium on Combustion*, Combustion Inst., Pittsburgh, PA, 1965, pp. 817–830.
[126] Vasiliev, A. A., *Gas Detonation of a Free Mixture Column*, Lavrent'yev Institute of Hydrodynamics, Siberian Branch of the USSR Academy of Sciences, Novosibirsk, 1980.
[127] Edwards, D. H., Thomas, G. O., and Nettleton, M. A., "The Diffraction of a Planar Detonation Wave at an Abrupt Area Change," *Journal of Fluid Mechanics*, Vol. 95, 1979, pp. 79–96.
[128] Murray, S. B., and Lee, J. H., "The Influence of Physical Boundaries on Gaseous Detonation Waves," *Dynamics of Explosions*, edited by

Bowen, J. R., Leyer, J. C., and Soloukhin, R. I., Vol. 106, Progress in Astronautics and Aeronautics, AIAA, New York, 1986, pp. 329–355.

[129] Zhang, F., "Detonation Waves in Dust Media: A Review," AIAA Paper 2002-0772, 2002.

[130] Gogulya, M. F., Makhov, M. N., Dolgoborodov, A. Yu., Brazhnikov, M. A., Arkhipov, V. I., and Shchetinin, V. G., "Mechanical Sensitivity and Detonation Parameters of Aluminized Explosives," *Fizika Goreniya Vzryva*, Vol. 40, 2004, pp. 82–95.

[131] Craven, A. D., and Greig, T. R., "The Development of Detonation Over-Pressures in Pipelines," *Chemical Engineering Symposium*, Series 25, 1968, pp. 41–50.

[132] Kogarko, S. M., "Investigation of the Pressure at the End of a Tube in Connection with Rapid Nonstationary Combustion," *Soviet Physics—Technical Physics*, Vol. 28, 1958, pp. 2041.

J. Powers
Associate Editor